Ward-constrained melonic renormalization group flow for the rank-four ϕ^6 tensorial group field theory

Vincent Lahoche[1,*] and Dine Ousmane Samary [ID][1,2,†]

[1]*Commissariat à l'Énergie Atomique (CEA, LIST), 8 Avenue de la Vauve, 91120 Palaiseau, France*
[2]*Faculté des Sciences et Techniques (ICMPA-UNESCO Chair), Université d'Abomey-Calavi,
072 B.P. 50, Cotonou, Benin*

The nontrivial fixed point discovered for ϕ^4-marginal couplings in tensorial group field theories has been shown to be incompatible with Ward-Takahashi identities. In a previous analysis, we have stated that the case of models with interactions of order greater than four could probably lead to a fixed point compatible with local Ward identities. In this paper, we focus on a rank-4 Abelian ϕ^6-just-renormalizable tensorial group field theory and describe the renormalization group flow over the subtheory space where the Ward constraint is satisfied along the flow, by using an improved version of the effective vertex expansion. We show that this model exhibits a nontrivial fixed point in this constrained subspace. Finally, the well-known asymptotically freedom of this model is highlighted.

I. INTRODUCTION

Group field theories (GFTs) are a type of nonlocal field theories defined on d copies of a group manifold. For more than a decade, they have been considered as a promising way to quantize gravity [1–6]. A well-defined theory for quantum gravity is necessary to understand the nature of space, time, and geometry and especially to address questions about the origins of our Universe. Indeed, the current description remains incomplete and fails at the Planck scale $\ell_p = \sqrt{G\hbar/c^3}$ because of the incompatibility between general relativity and quantum theory [7]. In the past years, some important developments were given in various directions to think about the question of quantum gravity, such as random geometry, canonical quantum gravity, and the covariant approach with spin-foam models, which have together converged toward the definition of GFTs [8–17]. In particular, GFTs provide a unified and convenient field theoretical framework to discuss the second quantization of loop quantum gravity (LQG) states, and their Feynman amplitudes coincide with spin-foam amplitudes, with a canonical weight [18–26]. Tensorial group field theories (TGFTs) are an improvement of the standard GFTs, including tensoriality as a strong criterion

to build interactions [27–33]. Tensoriality comes from colored random tensors models (RTMs) and corresponds to a specific invariance with respect to internal unitary transformations [27–33]. RTMs provide a nice generalization of random matrix models and are viewed as a convenient formalism for studying random geometry for dimensions higher than two [33]. The first success of RTMs was the discovery by Gurau (in 2009) of a $1/N$ expansion for tensors, analogous to the 't Hooft expansion for matrix models from which the genus is being replaced by a nontopological invariant called Gurau's degree [27–32,33]. Tensoriality has been pointed out to be a very strong improvement, allowing one to define the renormalization group and renormalizable actions. Renormalization and renormalizability take place in a *geometrogenesis scenario* for space-time emergence [34–42]. In this scenario, the large-scale structure of space-time with respect to the Planck scale is describe as a GFT condensate, analogous to the Bose-Einstein condensates in bosonic many-body systems [20–25]. The renormalization group (RG) allows one to build effective field theories from an elementary scale and to understand dynamical phase transitions in statistical and quantum systems (see [43–80], and references therein). In this respect, it was considered as a very important tool to understand the condensation mechanism in GFT.

The RG equations describe how the effective actions move when quantum fluctuations higher than a reference running scale are integrated out, building a path from the deep UV scale toward the large IR scales [43–47]. The trajectories from UV to IR are described as a flow through the infinite-dimensional functional space of allowed actions, the theory space. Nonperturbative methods

---

[*]vincent.lahoche@cea.fr
[†]dine.ousmanesamary@cipma.uac.bj

to build the RG group exist in standard field theories, the most popular and tractable being the functional renormalization group (FRG) method, based on the Wetterich-Morris equation [45–47]. These standard tools have been successfully applied for TGFT, a success especially due to the flexibility and the simplicity of the formalism, allowing one to deal with the specific nonlocalities of the TGFT interactions. Nonperturbative RG equations are known to be difficult to solve for TGFT models, as well as in standard field theory. This is why a large part of the studies on this topic limit their investigation of the truncation approximation. Truncation consists of a systematic projection into a reduced dimensional phase space along which the flow equations may be solved analytically or numerically. This method has been performed for a very large class of models [62–69]. Interestingly, all of them reveal the occurrence of a nonperturbative fixed point in the *symmetric phase*, that is, as long as the vanishing mean field remains a good vacuum around which we can expand the flow equation. These fixed points play different roles but are crucial, both for UV consistency of the theory and to support the condensation scenario. For the first case, the UV fixed point ensures the UV completion of the models, which are stated to be asymptotically free (and in the worst cases asymptotically safe [66]). The IR fixed point, in contrast, corresponds to nontrivial sums of spin-foam amplitudes at a large scale and then are reminiscent of a phase transition behavior.

In the deep UV, instead of a crude truncation into the full theory space, a recent approach [76–80] proposes to solve the same question, by replacing the truncation by the effective vertex expansion (EVE) in the reduced phase space with a closure of the hierarchical system derived from the exact RG group equation. To be more precise, in the EVE approach, we make use of relevant and marginal coupling as drivers of the full RG flow in the deep UV and solve the RG equations, discarding all the irrelevant contributions. The resulting equations, moreover, keep the full momenta dependence of the vertex function, allowing one to investigate beyond the local potential approximation. This, in particular, plays an important role for the derivation of the anomalous dimension and provides a relevant correction with respect to the truncations. In addition to these closure relations, the Ward-Takahashi identities provide some constraints which have to be solved simultaneously with the flow equations, at the same level of approximation. Taking into account this constraint seems to modify the picture drawing from flow equations only, in particular, for the existence of non-Gaussian fixed points.

In this paper, we will investigate the Ward-constrained RG flow for a ϕ^6-just-renormalizable model in rank 4. This model has been well defined and studied in Refs. [34,36] (see also Ref. [41] in the case of a gauge-invariant model). The motivation to be interested in such a model is the following: Note that the existence of a non-Gaussian fixed point can be understood from the following heuristic

argument. As shown in Ref. [73], the TGFT Feynman amplitudes can be analytically continued with respect to the group dimension D: $U(1) \rightarrow U(1)^D$. The power counting then indicates that there are two just-renormalizable models in rank 4: the ϕ^6 melonic model in group dimension $D = 1$ that we will describe in Sec. II and which is asymptotically free and the formal quartic melonic model in dimension $D = 4/3$, which is also asymptotically free. Let $|\epsilon| \ll 1$. The one-loop beta function for the quartic melonic model in dimension $D = 4/3 - \epsilon$ may be straightforwardly computed from the exact RG equation (24) to get

$$\beta_\lambda^{(1)} = -3\epsilon\bar{\lambda} - 2\eta^{(1)}\bar{\lambda} + 4\bar{\lambda}^2\sqrt{\pi} + \mathcal{O}(\bar{\lambda}^2, \epsilon), \qquad (1)$$

$$\beta_{m^2}^{(1)} = -(2 + \eta^{(1)})\bar{m}^2 - 8\bar{\lambda}\sqrt{\pi} + \mathcal{O}(\bar{\lambda}^2, \epsilon), \qquad (2)$$

where $\bar{\lambda}$ and $\bar{m}^2$ refer to the renormalized and dimensionless melonic coupling and mass parameter, respectively, and the one-loop anomalous dimension $\eta^{(1)}$ is given by

$$\eta^{(1)} = 4\bar{\lambda}\sqrt{\pi}. \qquad (3)$$

Equations (1) admit a nontrivial fixed point for the values

$$\bar{\lambda}_* = -\frac{3\epsilon}{4\sqrt{\pi}}, \qquad \bar{m}_*^2 = 3\epsilon. \qquad (4)$$

Now, let us consider the Ward constraint. From the results in Refs. [76–78], recalled in Sec. III C, the Ward identities enforce a relation between beta functions and the anomalous dimension. However, at one-loop order, this relation reduces to

$$\beta_\lambda^{(1)} = -3\epsilon\bar{\lambda} - \eta^{(1)}\bar{\lambda} + \mathcal{O}(\bar{\lambda}^2, \epsilon), \qquad (5)$$

which is nothing but the first equation (1). At one loop, and at the first order in ϵ, the non-Gaussian fixed point (4) is then compatible with the Ward identities. This fixed point has an attractive and a repulsive eigendirection in the UV, as qualitatively illustrated in Fig. 1, but it has the "wrong sign," a negative coupling which is able to break down the boundedness of the effective action. However, we have to keep in mind that $\epsilon \neq 0$ increases the strength of the inessential couplings; as a result, if such a formal fixed point survives in the limit $\epsilon \rightarrow 1/3$, when the ϕ^6 couplings become marginal, it may be viewed as a UV attractive fixed point ensuring UV completion of the RG flow. The same phenomena has been pointed out in Ref. [73]. However, the aim of this paper is to determine if such a fixed point remains compatible with Ward identities, by describing the flow at all orders in the coupling and the parameter ϵ and by using the EVE approach to solve the nonperturbative RG equation.

The outline of this paper is the following. In Sec. II, we describe the model and argue in favor of a reduced family of ϕ^6 couplings called *nonbranched*. In Sec. III, we use the EVE method to solve the nonperturbative RG equation.
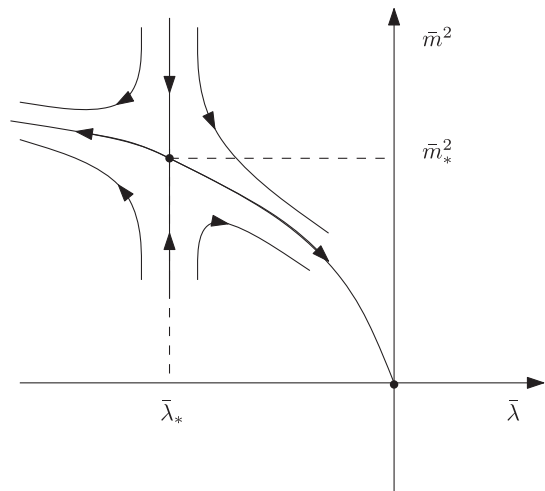
FIG. 1. A qualitative description of the non-Gaussian fixed point in the ϵ expansion.

Finally, in Sec. IV, we briefly describe the RG flow in the vicinity of the Gaussian fixed point, allowing one to recover the asymptotic freedom property. We then improve our analysis by implementing the so-called Ward-constraint melonic flow and conclude that one new nontrivial fixed point can be found on this subspace.

II. MICROSCOPIC MODEL AND NONPERTURBATIVE RG

As mentioned in the introduction, a GFT is a field theory whose fields are defined over d copies of a group manifold G. In this paper, we focus on the d-dimensional torus and

set $G = U(1)$, for a class of theories describing one complex field $\phi, \bar{\phi} : U(1)^d \to \mathbb{C}$ with the free action:

$$S_{\text{kin}}[\phi, \bar{\phi}] = \int_{G^d} d\mathbf{g} \bar{\phi}(\mathbf{g})(-\Delta_{\mathbf{g}} + m^2)\phi(\mathbf{g}), \qquad (6)$$

where $\mathbf{g} := (g_1, \ldots, g_d) \in G^d$ and where $\Delta_{\mathbf{g}}$ is the Laplace-Beletrami operator. For TGFTs, the interaction part is built as a sum of *connected tensorial invariants* called bubbles. A bubble involves the same number of fields ϕ and $\bar{\phi}$, such that any variable of a field ϕ is contracted with the corresponding variable of a field $\bar{\phi}$, ensuring a proper unitary invariance per contracted indices. The elementary example is a masslike term:

$$\int d\mathbf{g} \bar{\phi}(g_1, g_2, \ldots, g_d)\phi(g_1, g_2, \ldots, g_d). \qquad (7)$$

For higher-order interactions, we make use of a convenient graphical notation. To each field ϕ (respectively, $\bar{\phi}$), we associate a white (respectively, black) node, with d-colored half edges hooked to it. Each of these colored edges corresponds to the group arguments, and the colors to their labels. For a given number of white dotes, the allowed interactions correspond to the number of different ways to hook the edges of the black and white nodes together, following their respective colors. As a result, each bubble may be graphically pictured as a d-colored bipartite regular graph, and the interaction part of the classical action is in full generality written as

$$S_{\text{int}}[\phi, \bar{\phi}] = g_1 \; \vcenter{\hbox{}} \; + \; g_2 \; \vcenter{\hbox{}} \; + \; g_3 \; \vcenter{\hbox{}} \; + \; g_4 \; \vcenter{\hbox{}} \; + \cdots \qquad (8)$$

It should be noted that, in the ϕ_4^6 terminology, the number 4 corresponds to the rank of the tensors ϕ and $\bar{\phi}$, i.e., the dimension d. On the other hand, the number 6 is the maximal valence of the interactions. The spectrum of the Laplace-Beletrami operator introduces a canonical notion of scale, allowing one to build a renormalization group for this class of theory. This work has been done in a series of different works since 2012 [34–42], investigating perturbative and nonperturbative aspects. The most difficulty with respect to standard quantum field theories or statistical models comes from the specific nonlocality of the TGFT interactions. In order to deal with this specificity, an appropriate notion of locality has been addressed [40].

Definition 1.—For tensorial group field theories, connected bubbles are said to be local interactions.

The Feynman graphs $\mathcal{G}$ indexing the amplitudes of the perturbation theory are 2-simplex, i.e., a set of vertices, edges, and faces: $\mathcal{G} := (\mathcal{V}, \mathcal{L} \cup \mathcal{L}_{\text{ext}}, \mathcal{F} \cup \mathcal{F}_{\text{ext}})$, respectively, with cardinality V, L, L_{ext}, F, and F_{ext}. The sets of edges and faces split into internal and external subsets, respectively, without an index and with index "ext." For this, let us recall the definition of a face.

Definition 2.—A face is a maximal bicolored subset of edges, including necessarily the color zero awarded from the Wick contractions. The subset can be closed and/or opened, respectively, for closed and open faces.

For TGFTs as for any quantum field theory, perturbative amplitudes are indexed by Feynman graphs. The power counting has been established [34], and the superficial degree of divergence $\omega(\mathcal{G})$ corresponding to the graph $\mathcal{G}$ is

$$\omega(\mathcal{G}) := -2L(\mathcal{G}) + F(\mathcal{G}). \qquad (9)$$

The power counting allows one to classify the theories following their renormalizability. For a given order in the perturbation expansion, the optimal graphs with respect to the power counting (9) are called *melonics*. They are the graphs having the greatest number of faces by fixing L, and one can show that for melonic diagrams the three numbers V, L, and F are related as

$$F = (d-1)(L - V + 1). \qquad (10)$$

Denoting $\rho := (d-1)(L - V + 1) - F \geq 0$, the power counting may be rewritten as

$$\omega(\mathcal{G}) = \sum_k ((d-3)k - (d-1))v_k(\mathcal{G}) + (d-1)$$
$$- \frac{N(\mathcal{G})}{2}(d-3) - \rho(\mathcal{G}), \qquad (11)$$

where v_k denotes the number of bubbles valence $2k$ (i.e., having k white nodes) and $N(\mathcal{G}) = N$ is the number of external edges of the graph $\mathcal{G}$. For melonic diagrams, $\rho(\mathcal{G}) = 0$. The theory is said to be just renormalizable if and only if $(d-3)k - (d-1) \leq 0$, the maximal valence being $k_0 = (d-1)/(d-3)$. In particular, for $d = 4$, we get $k_0 = 3$. The power counting suggests the existence of a just-renormalizable model involving ϕ^6 interactions, with

$$\omega(\mathcal{G}) = -2v_1(\mathcal{G}) - v_2(\mathcal{G}) + 3 - \frac{N(\mathcal{G})}{2} - \rho(\mathcal{G}). \qquad (12)$$

For $\rho = 0$, only melonic diagrams with $N \leq 6$ are divergent. Moreover, one can easily show that $\rho \geq 1$, implying that, for $N \geq 4$, all the superficially divergent diagrams are melonics; see Ref. [34]. An example of two-point superficially subleading divergent graph is given in Fig. 2. From
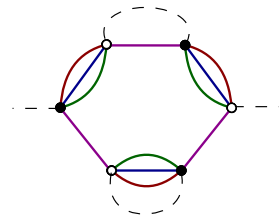

FIG. 2. A subdivergent two-point diagram built from a six-point vertex. The dotted edges correspond to the Wick contractions. From a direct computation, $\omega = -2 \times 2 + (3 + 1) = 0$.

the locality principle, Definition 1, the divergent subgraphs can be subtracted with local counterterms. The procedure may be extended successfully to all orders of the perturbative expansion, allowing one to prove a solid renormalizability theorem [34–42].

Let $\mathcal{G}$ be a melonic diagram, and then its vertex bubbles have to be melonic. We recall briefly the definition of the melonic bubbles.

Definition 3.—Any melonic bubble b_ℓ of valence ℓ may be deduced from the elementary melon b_1:

$$(13)$$

replacing successively $\ell - 1$ colored edges as follows, defining the insertion operator $\mathfrak{R}_i$:

$$(14)$$

Then $b_\ell := (\prod_{\alpha=1}^{\ell-1} \mathfrak{R}_{i_\alpha}) b_1$.

The melon graphs were introduced in the colored random tensor models, where they arise as leading-order graphs in the $1/N$ expansion.[1] This expansion is characterized with an exponent ϖ playing the same role as the genus for random matrices, the *Gurau degree*, vanishing for melons. The Abelian ϕ_4^6-melonic model,[2] defined with the classical action

$$S[\phi, \bar{\phi}] = S_{\text{kin}}[\phi, \bar{\phi}] + \lambda_4 \sum_{i=1}^4 \boxed{i} + \lambda_{6,1} \sum_{i=1}^4 \boxed{i} + \lambda_{6,2} \sum_{i<j} \boxed{\begin{matrix}i\\j\end{matrix}}, \qquad (15)$$

has been shown to be just renormalizable, and a Bogoljubow-Parasjuk-Hepp-Zimmermann (BPHZ) theorem has been also proved [34].

The renormalization group flow describes the change of the couplings in the effective action when UV degrees of freedom are integrated out. The FRG formalism is a

---

[1]Remark that in the terminology "$1/N$ *expansion*" N refers to the size of the tensors but is not the number of external edges of the graph $\mathcal{G}$ which is also denoted by N.

[2]The expression "melonic" referred to the leading-order contribution; i.e., the partition and correlation functions admit perturbative expansions which are dominated by peculiar triangulations of spheres called melons.

specific way to build such an evolution in the theory space of all possible actions. It has been shown to be a promising theoretical framework for tensorial field theory, allowing one to deal with the specific nonlocality of the interactions and to investigate the nonperturbative regime. In the FRG formalism, the quantum model is described by a one-parameter family of partition functions $\{\mathcal{Z}_k\}$, $k \in \mathbb{R}$, from a microscopic action S in the deep UV ($k = \Lambda$) to an effective action Γ in the deep IR ($k = 0$). For just-renormalizable models, the microscopic scale Λ becomes irrelevant and may be removed in the continuum limit $\Lambda \to \infty$. If k walks around the interval $[\Lambda, 0]$, we run through successive effective models, with effective average action Γ_k. The step partition function $\mathcal{Z}_k(J, \bar{J})$ is defined as

$$\mathcal{Z}_k(J, \bar{J}) := \int d\phi d\bar{\phi} e^{-S[\phi,\bar{\phi}]-R_k[\phi,\bar{\phi}]+\bar{J}\cdot\phi+\bar{\phi}\cdot J} \quad \forall \ k \in [0, \Lambda],$$

(16)

where $a \cdot b := \int d\mathbf{g} a(\mathbf{g}) b(\mathbf{g})$. The driving or *coarse graining* along the RG flow is ensured by the regulator function $R_k[\phi, \bar{\phi}]$, which behaves like a momentum-dependent mass term:

$$R_k[\phi, \bar{\phi}] := \int d\mathbf{g} \bar{\phi}(\mathbf{g}) r_k(-\Delta) \phi(\mathbf{g}),$$

(17)

ensuring that the UV degrees of freedom with respect to the running scale k are integrated out, with boundary conditions:

$$\Gamma_{k=\Lambda} = S, \qquad \Gamma_{k=0} = \Gamma.$$

(18)

The regulator $r_k(-\Delta)$ depends on the spectrum values of the Laplace-Beletrami operator and is positive defined. For convenience, we work in the momentum representation, the Fourier components of the fields ϕ and $\bar{\phi}$ becoming discrete tensors on $\mathbb{Z}^4$:

$$\phi(g_1, g_2, g_3, g_4) = \sum_{\vec{p} \in \mathbb{Z}^4} T_{p_1, p_2, p_3, p_4} e^{i \sum_j p_j \theta_j},$$

$$\bar{\phi}(g_1, g_2, g_3, g_4) = \sum_{\vec{p} \in \mathbb{Z}^4} \bar{T}_{p_1, p_2, p_3, p_4} e^{-i \sum_j p_j \theta_j},$$

(19)

the θ coordinates being angle variables $\theta_j \in [0, 2\pi[$, such that $g_j = e^{i\theta_j}$. In Fourier representation, r_k becomes a function of the square of the momentum only, having generically the following structure:

$$r_k(\vec{p}^2) := k^2 f(\vec{p}^2/k^2).$$

(20)

The function f has to be positive defined as well and has to satisfy some requirements with respect to the boundary conditions (18), among which
  (1) $\lim_{k \to \Lambda} r_k(\vec{p}^2) \gg 1$,
  (2) $\lim_{k \to 0} r_k(\vec{p}^2) = 0$,
  (3) $r_k(\vec{p}^2 > k^2) \simeq 0$.

The effective average action Γ_k is defined as a slightly modified Legendre transform of the free energy $W_k := \ln \mathcal{Z}_k$:

$$\Gamma_k[M, \bar{M}] + R_k[M, \bar{M}] = \bar{J} \cdot M + \bar{M} \cdot J - W_k[J, \bar{J}], \quad (21)$$

where the mean fields M and $\bar{M}$ are themselves tensor fields, defined, respectively, as

$$M_{\vec{p}} := \frac{\partial W_k}{\partial \bar{J}_{\vec{p}}}, \qquad \bar{M}_{\vec{p}} := \frac{\partial W_k}{\partial J_{\vec{p}}}.$$

(22)

The presence of the R_k term in the definition (21) enforces the initial condition $\Gamma_{k=\Lambda} = S$. Moreover, it means that the effective two-point function G_k has to be related with the second derivative of the effective action, i.e., $\Gamma_k^{(2)} := \partial_M \partial_{\bar{M}} \Gamma_k$, as:

$$G_k(\vec{p}, \vec{p}') := (\Gamma_k^{(2)} + r_k \mathbb{I})^{-1}(\vec{p}, \vec{p}'),$$

(23)

where $\mathbb{I}$ designates the identity matrix. The effective average action moves through the theory space with the running scale k, and its evolution obeys the exact flow equations known as *Wetterich-Morris equations*:

$$\dot{\Gamma}_k = \sum_{\vec{p} \in \mathbb{Z}^4} \dot{r}_k(\vec{p}^2)(\Gamma_k^{(2)} + r_k \mathbb{I})^{-1}(\vec{p}, \vec{p}),$$

(24)

where the dot designates the derivative with respect to the normal coordinate along the flow curves: $s := \ln k$. Despite its simplicity, this equation is very difficult to solve exactly and requires appropriate approximation schemes. This difficulty may be tracked by taking in the Wetterich equation the successive derivations with respect to the mean fields M and $\bar{M}$, generating an infinite hierarchical system of coupled equations. For TGFTs, the nonlocality of the interactions introduces a substantial difficulty, discarding some powerful tools used for standard quantum fields. Until recent years, only the *truncation method*, which stops crudely the hierarchical system, seemed to be relevant to solve Eq. (24). Some progress in solving the flow equation beyond the truncation method has been made in a series of recent works [76–80]. The method, called EVE, allows one to truncate "smoothly" the infinite hierarchical system, closing it around marginal operators. The strategy is to use relevant and marginal operators to drive the flow of the highest-order effective vertices, all expressed in terms of a reduced set of effective functions. In this approach, moreover, a fixed point for the reduced system has to be as well a global fixed point. Until now, there are four limitations for this method. First of all, it works well only in the UV sector $\Lambda \gg k \gg 1$, where only leading-order contributions survive. This condition plays an important role, the properties of the leading sector being used to close the hierarchical system. Second, it seems difficult to use it for branching interactions like the interaction associated with the coupling $\lambda_{6,2}$ in Eq. (15). Third, the

method is difficult to extend for the highest order of the derivative expansion. Finally, the EVE method has not been applied beyond the *symmetric phase*, where the mean fields vanish. Among the relevant properties of the region of the phase space reached from an expansion around $M = \bar{M} = 0$, we mention the following, discussed in Refs. [77–79].

Property 1.—In the symmetric phase, all the odd effective vertex functions not having the same number of derivatives with respect to M and $\bar{M}$ vanish. Moreover, the effective two-point function $G_k(\vec{p}, \vec{p}')$ is diagonal:

$$G_k(\vec{p}, \vec{p}') := G_k(\vec{p})\delta(\vec{p}, \vec{p}'). \qquad (25)$$

To fix the initial conditions, we restrict our attention to the nonbranching sector, defined as follows.

Definition 4.—A nonbranching melonic bubble of valence ℓ, $b_\ell^{(i)}$ is labeled with a single index $i \in [\![1, 4]\!]$ and defined such that

$$b_\ell^{(i)} := (\mathfrak{R}_i)^{\ell-1} b_1. \qquad (26)$$

Figure 3 provides the generic structure of melonic nonbranching bubbles.

As mentioned before, the method we consider in this paper to deduce the flow equations works well only for the nonbranching sector. The same point has been discussed for another family of graphs called *pseudomelons* in

Ref. [79], and it is a first source of limitation for our incoming conclusions. The interest of this sector in the fixed point investigation has been pointed out in Ref. [66] for a non-Abelian TGFT over $SU(2)^3$ with a closure constraint. Because we expect that the UV behavior of this model and the model defined by the action (15) are the same, the restriction to the nonbranching sector seems to be not so bad as a starting condition. There is another interest for this restriction, justifying the terminology "sector." In the UV domain $\Lambda \gg k \gg 1$, the corresponding reduced theory space is stable under the renormalization group transformations. Indeed, deriving the flow equation (24) with respect to M and $\bar{M}$, and from Property 1, we get that the flow equation for $\Gamma_k^{(n)}$ involves $\Gamma_k^{(n+2)}$, $\Gamma_k^{(n)}$, and the smallest effective vertices. All these effective vertices can be labeled with a bubble drawing the pattern following which external momenta are pairwise identified and corresponding to the *boundary graph* of the relevant Feynman graphs involved in perturbative expansion of these effective vertex functions. From a direct inspection, it can be easily checked recursively that, starting with effective vertices indexed with nonbranching melonic bubbles as building blocks, we do not generate leading-order one-loop contributions outside of the nonbranching subspace. The calculations of Sec. III A support explicitly this argument.

From these considerations, the microscopic action S, fixed for some fundamental UV scale Λ, is the following:

$$S[T, \bar{T}] = \sum_{\vec{p} \in \mathbb{Z}^d} \bar{T}_{\vec{p}} \left(Z_{-\infty} \vec{p}^2 + Z_2 m_0^2 \right) T_{\vec{p}} + Z_4 \lambda_4 \sum_{i=1}^{4} \boxed{i} \; + Z_6 \lambda_6 \sum_{i=1}^{4} \hexagon_i \;, \qquad (27)$$

where $Z_{-\infty}$, Z_2, Z_4, and Z_6 denote, respectively, the wave function, mass, and coupling counterterms. From the renormalizability theorem, they allow one to cancel all the divergences occurring in the perturbative expansion. In the standard nonperturbative RG analysis, these counterterms are not explicitly introduced, and the choice of the initial conditions is not extensively discussed. The reason why we discuss them has been explained in a recent work [80] for a melonic ϕ^4 model. The nonperturbative equation (24) is divergence free due to the regulator function $\dot{r}_s$. However, we will discuss the compatibility between flow equations and Ward identities; and some UV divergences occurs in them, as a consequence of the

nonlocality of the interactions. Counterterms are then essential to deal with these specific divergences. The index "$-\infty$" refers to the fact that the finite part of the counterterms in fixed in the deep infrared limit $k \to 0$ or $s \to -\infty$. Note that the limit may be formal and simply means that it is chosen for very small k, i.e., at a scale so far from the domain $k \ll 1$.

To conclude this section, we provide some central notion for our analysis called the *canonical dimension*. In standard quantum field theories (QFTs), the dimension of the interactions is closely related with their renormalizability. Interactions with positive or vanishing (momentum) dimensions are renormalizables, while the ones with negative
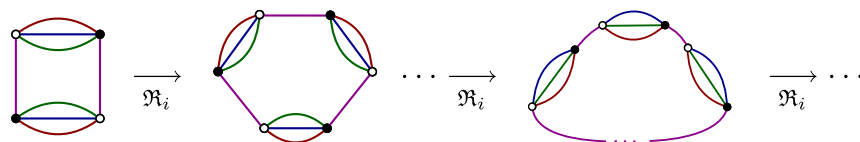

FIG. 3. Structure of the nonbranching melons, from the smallest one b_2.

dimensions are nonrenormalizables. For GFTs, however, the situation is more subtle. There is no reference scale in the classical action (27), and the sums over $\mathbb{Z}^d$ are dimensionless in contrast with integrations over space-time in the ordinary QFT. There are two ways to introduce a dimension in the GFT framework and recover the standard classification following the dimension of the couplings. The first one is to make contact with physical quantities. In particular, for non-Abelian models over SU(2), the spectrum of the Laplacian may be related with the size of the area operator in LQG, and the result can be extended for Abelian cases. The second strategy is to fix the dimension from the renormalization group flow. Indeed, the leading-order scaling of the operators with respect to the UV cutoff may be viewed as a dimension; and from the definition of a just-renormalizable model, one expect that just-renormalizable interactions scale logarithmically with the cutoff and then have zero dimension. For melonic diagrams in the UV, one can easily check the canonical dimension of the operators from the power-counting law (9). Any leading-order N-point functions built only with six-point interactions scale as

$$\omega = 3 - \frac{N}{2}. \qquad (28)$$

In particular, the proper scaling of the leading-order six-point functions vanishes, meaning that it scales logarithmically with the UV cutoff. Following the definition of the canonical dimension as the leading-order scaling of the quantum corrections, it makes sense to associate a dimension zero for the coupling λ_6. For the same reason, setting $N = 4$, the dimension of the coupling λ_4 has to be 1. Indeed, from the definition of renormalizability, we expect a proliferation of just-renormalizable interactions, which have to fix the leading scaling. Note that this condition is compatible with the "cost" -1 of the ϕ^4 melonic bubbles in the power counting (9). Finally, the dimension of the mass parameter has to be 2. For interactions with valence $N/2$, the canonical dimension is explicitly given from formula (28). We then recover the standard classification, renormalizable interactions having a positive dimension and nonrenormalizable ones having a negative dimension. For an extended discussion, the reader may consult Ref. [39].

III. SOLVING THE RG EQUATION IN THE NONBRANCHING SECTOR

In this section, we solve the exact flow equation (24) using the EVE approximation scheme introduced in Refs. [76–80]. The melonic model that we consider being very close to the nonbranching pseudomelonic sector discussed in Ref. [78], we give only the main steps of the proof. As explained in the previous section, the strategy is to close the hierarchical system of coupled equations deduced from Eq. (24), that is, to explain the effective vertex $\Gamma_k^{(8)}$ in terms

of $\Gamma_k^{(6)}$, $\Gamma_k^{(4)}$, and $\Gamma_k^{(2)}$, using the essential and marginal couplings to drag the RG flow of the highest effective vertices. Moreover, the method goes beyond a "smooth" truncation, in the sense that EVE allows one to capture the momentum dependence of the effective vertex, which plays the role of the anomalous dimension. To be more precise, the Ward identity allows one to compute the momentum derivative of the effective four-point vertices in term of the marginal and essential couplings, improving the crude truncation which does not consider this additional contribution. Indeed, as pointed out in Ref. [76], taking into account the momentum dependence of the four-point vertex leads to discarding a line of singularity and to extending maximally the symmetric phase region. We start from the derivation of the hierarchical equations in the nonbranching melonic sector up to six-point effective local vertices. For a second time, we build the structure equation for the $\Gamma_k^{(8)}$ vertex and use Ward identities to compute the derivative of the effective four-point vertex. As a result, we get a set of four autonomous coupled equations, involving only relevant and marginal dimensionless couplings. Finally, we discuss an additional constraint coming from the Ward identity linking $\Gamma_k^{(4)}$ and $\Gamma_k^{(2)}$. As pointed out in Ref. [76], in the deep UV, this equation may be turned locally in the flow as a constraint linking beta functions for four- and two-point relevant and marginal couplings. This additional constraint has to be solved simultaneously with the flow equations, reducing the dimension of the phase space from three to two.

A. RG equations for marginal local couplings

Deriving for the first time with respect to M and $\bar{M}$ the exact flow equation (24), we get an equation for $\dot{\Gamma}^{(2)}$, involving $\Gamma^{(4)}$ and $\Gamma^{(2)}$:

$$\dot{\Gamma}_k(\vec{p}) = -\sum_{\vec{q} \in \mathbb{Z}^d} \Gamma_k^{(4)}(\vec{p}, \vec{p}, \vec{q}, \vec{q}) \dot{r}_k G_k^2(\vec{q}), \qquad (29)$$

where we used Property 1. As explained in the previous section, the effective vertex function may be indexed with a nonbranching bubble corresponding to the boundary of the graphs indexed with the amplitudes in their perturbative expansion. For nonbranching bubbles, these boundaries are indexed with a single index. Then, as a consequence, the nonbranching effective vertices $\Gamma^{(n)}$, for $n > 2$, decompose as

$$\Gamma_k^{(2n)} = \sum_{i=1}^{d} \Gamma_k^{(b_n^{(i)})}. \qquad (30)$$

The structure of the partial n-point functions $\Gamma_k^{(b_n^{(i)})}$ has been extensively discussed in Ref. [76]. The boundary graph dictates the ways to identify external momenta. Formally, it corresponds to a product of Kronecker deltas following the

path drawn by the corresponding bubble interaction. To simplify the notations, we represent these products of deltas with d-colored regular bipartite graphs as well, indexed with external momenta. For instance,

$$= \delta_{p_{1i}p_{4i}} \delta_{p_{2i}p_{3i}} \prod_{j \neq i} \delta_{p_{1j}p_{2j}} \delta_{p_{3j}p_{4j}}, \qquad (31)$$

$$= \delta_{p_{1i}p_{6i}} \delta_{p_{2i}p_{3i}} \delta_{p_{4i}p_{5i}} \prod_{j \neq i} \delta_{p_{1j}p_{2j}} \delta_{p_{3j}p_{4j}} \delta_{p_{5j}p_{6j}}. \qquad (32)$$

The partial effective vertex functions $\Gamma_k^{(b_n^{(i)})}$ then may be written as

$$\Gamma_k^{(b_n^{(i)})}(\{\vec{p}_\ell\}) =: \pi_k^{(b_n^{(i)})}(p_{\ell\,i}) \times \text{Sym} \left(\text{} \right), \qquad (33)$$

where Sym denotes the permutation of the external momenta. For instance,

$$\text{Sym} \left(\text{} \right) = 2 \left(\text{} + \text{} \right), \qquad (34)$$

the factor 2 coming from the fact that permuting both the black and white nodes does not change the configuration. The kernels $\pi_k^{(b_n^{(i)})} : \mathbb{Z}^n \to \mathbb{R}$ depend on the ith component of the external momenta. The zero-momenta values of the effective vertex functions are related with the effective coupling constants at scale k. For relevant and marginal couplings, we set

$$\Gamma_k^{(2)}(\vec{0}) =: m^2(k), \qquad \Gamma_k^{(4)}(\{\vec{0}\}) =: (2!)^2 \lambda_4(k), \qquad \Gamma_k^{(6)}(\{\vec{0}\}) =: (3!)^2 \lambda_6(k), \qquad (35)$$

the k dependence on the couplings allowing one to differentiate them from the "bare" couplings. From definition of the kernels $\pi_k^{(b_n^{(i)})}$, we have therefore $\pi_k^{(b_2^{(i)})}(0) = \lambda_4(k)$ and $\pi_k^{(b_3^{(i)})}(\{0\}) = \lambda_6(k)$. For the rest of this section, we left the arguments for zero-momenta functions when it is unambiguous. Inserting the decomposition (30) in the flow equation (29), we get, graphically,
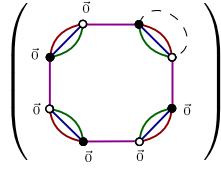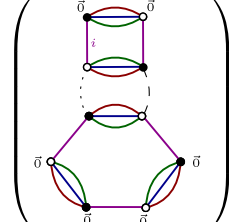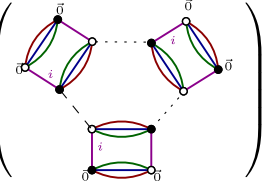
$$\dot{\Gamma}_k(\vec{p}) = -2 \sum_{i=1}^{d} \pi_k^{(b_2^{(i)})}(p_i) \left(\text{} + \text{} \right) \approx -2 \sum_{i=1}^{d} \pi_k^{(b_2^{(i)})}(p_i) \left(\text{} \right), \qquad (36)$$

where the dashed line corresponds to the contraction with the propagator $\dot{r}_k G_k^2$. For the last term, we kept only the melonic contractions, creating three internal faces, the second contribution having a relative scaling k^{-2} with respect to the melonic one and may be discarded in the UV

sector $k \gg 1$. The rule follows as soon as we remain in this domain; and for higher-order interactions we will keep only the melonic contraction. We get, for $\Gamma_k^{(4)}$ and $\Gamma_k^{(6)}$, taking successive derivatives of Eq. (24) and vanishing their external momenta, from renormalization conditions (35):

$$(2!)^2\dot{\lambda}_4 = -12\pi_k^{(b_3^{(1)})}\left(\text{}\right) + 4\times(2!)^2\big(\pi_k^{(b_2^{(1)})}\big)^2\left(\text{}\right), \tag{37}$$
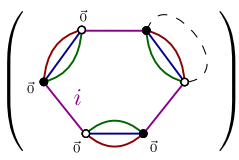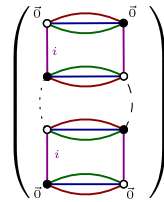
where the dotted line on the last diagram corresponds to the contraction with the effective propagator G_k. All the numerical coefficients count the number of independent melonic contractions or arise from the derivation of Eq. (24). This is the case of the factor 4, which is in fact $2+2$: a first factor 2 coming from the derivation of G_k^2 in Eq. (29) and a second factor 2 coming from an odd term, discarded in the calculation of Eq. (29). In the same way,

$$(3!)^2\dot{\lambda}_6 = -4\times(3!)^2\pi_k^{(b_4^{(1)})}\left(\text{}\right) + 2(3!)^3\pi_k^{(b_3^{(1)})}\pi_k^{(b_2^{(1)})}\left(\text{}\right)$$

$$-2^3(3!)^2\big(\pi_k^{(b_2^{(1)})}\big)^3\left(\text{}\right). \tag{38}$$

The mass flow may be fixed from the renormalization conditions (35), setting $\vec{p}=\vec{0}$ on both sides of Eq. (29). All the diagrams may be easily computed. They involve only a single loop, creating three internal faces. Denoting as p the external momentum running through the external face of color i, the explicit expression for the loop of length j, $L_j(p)$ is written as

$$L_j(p) := \sum_{\vec{q}\in\mathbb{Z}^4}\delta_{q_1 p}\,\dot{r}_k G_k^{j+1}(\vec{q}). \tag{39}$$

Therefore, Eqs. (36)–(38) may be written explicitly as follows:

$$\dot{m}^2 = -2\lambda_4 L_1(0), \tag{40}$$

$$\dot{\lambda}_4 = -3\lambda_6 L_1(0) + 4\lambda_4^2 L_2(0), \tag{41}$$

$$\dot{\lambda}_6 = -4\pi_k^{(b_4^{(1)})}L_1(0) + 12\lambda_4\lambda_6 L_2(0) - 8\lambda_4^3 L_3(0), \tag{42}$$

where we denote $\dot{x} := k\frac{dx}{dk}$. To close the system, we have to express the remaining piece $\pi_k^{(b_4^{(1)})}$, the effective coupling with valence 4, in terms of the relevant and marginal couplings. This aims to understand independently the dependence of the four-, six-, and eight-point effective vertices with respect to the effective marginal and essential couplings at scale k. Investigating the structure of the leading perturbative Feynman graphs building the effective vertices, *assumed to be analytic functions of the effective couplings*, and from renormalization conditions defining effective couplings at scale k, we deduce some relations between effective vertices and renormalizable couplings. The assumption about analyticity of the effective vertex functions ensures the validity of these relations out of the perturbative domain, as long as we remain in the symmetric phase. Indeed, expanding around a nonzero vacuum breaks the diagonal condition given by Property 1, which is satisfied in the perturbative sector as well.

B. Closing hierarchy: The EVE method

In a first time we restrict our attention on the quartic sector, whose graphs building the effective functions are made with quartic melonic interactions only. We have the following proposition.

Proposition 1.—Let us denote as $\bar{\pi}_k^{(b_n^{(i)})}$ the leading-order effective vertices of valence n built of quartic melonic interactions only. For $n=2$, 3, and 4, their expressions in terms of the bare coupling $Z_4\lambda_4$ are the following:

$$\bar{\pi}_k^{(b_2^{(i)})} = \frac{Z_4\lambda_4}{1 + 2Z_4\lambda_4\mathcal{A}_{k,2}}, \qquad (43)$$

$$\bar{\pi}_k^{(b_3^{(i)})} = \frac{8}{3}(\bar{\pi}_k^{(b_2^{(i)})})^3 \mathcal{A}_{k,3}, \qquad (44)$$

$$\bar{\pi}_k^{(b_4^{(i)})} = -2(\bar{\pi}_k^{(b_2^{(i)})})^4 \mathcal{A}_{k,4} + \frac{16}{3}(\bar{\pi}_k^{(b_2^{(i)})})^5 (\mathcal{A}_{k,3})^2, \qquad (45)$$

where $\mathcal{A}_{k,n} \equiv \mathcal{A}_{k,n}(0)$, with

$$\mathcal{A}_{k,n}(p) := \sum_{\vec{q} \in \mathbb{Z}^4} \delta_{pq_1} G_k^n(\vec{q}). \qquad (46)$$

To prove this proposition, we recall the following lemma, already considered in Ref. [79].

Lemma 1.—Let $\mathcal{G}$ be a 1PI $2N$-points diagram with more than one vertex. It has N boundary vertices to which external edges are hooked, $d - 1$ external faces per external vertex, and N external faces of the same color running through the interior of the diagram.

Proof.—We will proceed recursively for each n, and we will indicates only the first steps of the proof. More details may be found in Ref. [79].

Four-point effective vertices.—Let us denote as $Z_4\lambda_4\Pi_4$ the part of $\bar{\pi}_k^{(b_2^{(i)})}$ made of at least two vertices. We have, setting $i = 1$,

$$\bar{\pi}_k^{(b_2^{(1)})} = Z_4\lambda_4(1 + \Pi_4). \qquad (47)$$

Let us consider the structure of Π_4. Taking into account the face connectivity and Lemma 1, the boundary vertices may be such that the two internal faces of the same color running on the interior of the diagrams building Π_4 pass through them. As a result, we expect the following structure, compatible with the boundary graph $b_2^{(1)}$:

$$(48)$$

where the gray disk indexed with $\bar{\Pi}_4$ is itself a sum of Feynman graphs. It is easy to verify that other configurations of the boundary vertices move away from the leading order. Extracting the one-particle irreducible part $\bar{\Pi}_4'$ of $\bar{\Pi}_4$, we get, graphically as well,

$$(49)$$

where the gray disks indexed by G denote the leading-order effective propagator *in the quartic sector* (we left the index k to simplify the figures). The remaining contribution Π_4' is at least of the order of 1, that is, built with a single vertex. Isolating this vertex, the next-order terms build an effective vertex made of 1PI graphs having at least two vertices, corresponding to that we called Π_4. As a result, it is easy to check the following closed equation:

$$(50)$$

which can be formally solved recursively as

$$(51)$$

Consider now Eq. (47), and we then get

$$(52)$$

where we used the following graphical conventions:

$$\equiv -Z_4\lambda_4. \qquad (53)$$

Finally, the effective one-loop diagram on the denominator of Eq. (52) may be easily computed recursively, leading to

$$= -2Z_4\lambda_4\,\mathcal{A}_{k,2}\,, \qquad (54)$$

which proves formula (43).

Six-point effective vertices.—From Lemma 1, the external edges have to be hooked to three vertices of the same type, sharing the three external faces of the same color

running through the interior of the diagrams building $\bar{\pi}_k^{b_3^{(1)}}$. We then expect the following structure:

$$\bar{\pi}_k^{b_3^{(1)}} = \qquad . \qquad (55)$$

As for four-point graphs, the kernel Π_6 may be decomposed into one-particle irreducible components as

$$\qquad (56)$$

The procedure may be conduct recursively like for the four-point functions. The perturbative expansion of the connected one-particle irreducible component Π_6' starts without a vertex, and a moment of reflection shows that it is nothing but Π_6 itself. Solving the recurrence, we get that each of the three arms reconstructs the structure of the effective four-point function, as a result:

$$\bar{\pi}_k^{b_3^{(1)}} = \qquad = K\left(\bar{\pi}_k^{(b_2^{(i)})}\right)^3\mathcal{A}_{k,3}\,, \qquad (57)$$

where the gray bubbles indexed with $\bar{\pi}_k^{b_2^{(1)}}$ represent effective four-point functions and where, for the last term, we translate the diagram into a formula. The remaining numerical factor K may be fixed from the leading order in the perturbative expansion. This term involves three vertices, each of them having two orientations; then we have $K = 2^4/3! = 8/3$.

Eight-point effective vertices.—As for four- and six-point functions, because of Lemma 1, we expect the following configuration for the boundary vertices:

$$\bar{\pi}_k^{b_4^{(1)}} = \qquad . \qquad (58)$$

Decomposing the kernel Π_8 following one-particle irreducible parts, we get

$$\qquad (59)$$

Note that Π_8'' is a one-particle irreducible function, at least of the order of one; and it is not hard to check that it is nothing but $\pi_k^{(b_2^{(1)})}$. Recursively, we get, as for a six-point function,

$$\bar{\pi}_k^{b_4^{(1)}} = \quad \text{} \quad + \quad \text{} \quad = -\frac{2^3 3!}{4!} \left(\bar{\pi}_k^{(b_2^{(i)})} \right)^4 \mathcal{A}_{k,4} + \frac{2^7}{4!} \left(\bar{\pi}_k^{(b_2^{(i)})} \right)^5 \left(\mathcal{A}_{k,3} \right)^2 . \tag{60}$$

∎

The structure equations in the full sector, including six-point vertices, must be easily deduced from Proposition 1. Let us recall that six-point vertices may be obtained as a connected sum of two four-point vertices using the following definition.

Definition 5.—Let $b_2^{(i)}$ and $b_2^{(j)}$ be two four-point bubbles. Let $n \in b_2^{(i)}$ and $\bar{n} \in b_2^{(j)}$ be two white and black nodes and e a dotted edge joining together the two nodes. The connected sum $b_2^{(i)} \sharp_{n\bar{n}} b_2^{(j)}$ is defined as the bubble obtained from the two following successive moves:

   (i) deleting the edge e and
  (ii) connecting together the colored edges hooked to n and $\bar{n}$ following their respective colors.

Figure 4 below provides an illustration.

The leading-order graphs in the full sector, including six-point vertices, can then be obtained from the leading-order graphs in the restricted quartic sector, contracting some edges between adjacent quartic vertices. From the definition, the contracted edges do not change the number of faces; moreover, each contraction does not change the power counting: Deleting an edge increases the power counting of 2, compensating exactly the loss of two quartic vertices, each of them with canonical dimension 1.

Let us consider a 1PI four-point graphs contributing to $\Gamma_k^{(4)}$, and e an edge between two adjacent vertices. We have to distinguish two cases:

   (i) The edge e is included into an effective propagator G_k.
  (ii) The edge e is between two consecutive vertices on the chain.

In the first case, the resulting two-point subgraph is nothing but a contribution to the full two-point function. In the second case, the contraction of the edge generates a six-point graph along the chain as follows:

$$\text{} \tag{61}$$

Two elementary quartic vertices have been replaced by an effective quartic vertex, building from an elementary six-point vertex by contracting two external fields with the effective propagator G_k to form an effective 3-dipole. Note

that the propagator G is becoming the full effective propagator, including six-point vertices as well. We call *type-2 quartic vertices* these new building blocks in the chain:
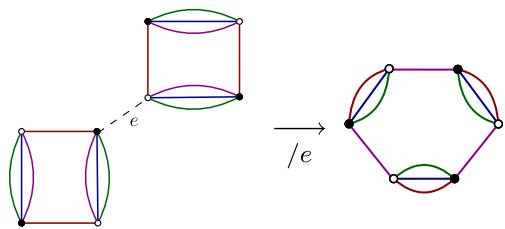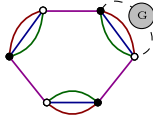
$$\text{} \tag{62}$$

and their explicit expression may be easily computed. For zero-external momenta, we get

FIG. 4. Connected sum of two quartic bubbles.

$$= Z_6 \lambda_6 \times \mathfrak{b}_k, \quad \mathfrak{b}_k := 3 \sum_{\vec{p} \in \mathbb{Z}^{d-1}} G_k(\vec{p}), \tag{63}$$

where $Z_6 \lambda_6$ denotes the bare six-point coupling and the factor 3 in the definition of $\mathfrak{b}_k$ comes from the counting of all possible contractions. The structure of the full chain, including six-point vertices, may be deduced exactly following the same strategy as for the proof of Proposition 1. Denoting as $\tilde{\pi}_k^{(b_2^{(1)})}$ the leading-order four-point effective kernel made of chains built only of type-2 quartic vertices, we get

$$\tilde{\pi}_k^{(b_2^{(1)})} = \frac{Z_6 \lambda_6 \mathfrak{b}_k}{1 + 2 Z_6 \lambda_6 \mathfrak{b}_k \mathcal{A}_{k,2}}. \tag{64}$$
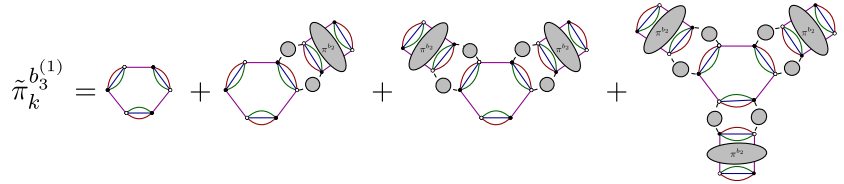
To find the full effective vertex, we have to take into account the proliferation of the two types of four-point vertices along the chain. There are three cases that we have to distinguish:

    (i) the boundary vertices are both of type 1,
    (ii) the boundary vertices are both of type 2, and
    (iii) the boundary vertices are assorted.

For the first case, starting with $\bar{\pi}_k^{(b_2^{(1)})}$, we may consider all the possible insertions of $\tilde{\pi}_k^{(b_2^{(1)})}$ without breaking the boundary constraint. We get

$$\bar{\pi}_k^{(b_2^{(1)})} + \bar{\pi}_k^{(b_2^{(1)})} \tilde{\pi}_k^{(b_2^{(1)})} \bar{\pi}_k^{(b_2^{(1)})} + \bar{\pi}_k^{(b_2^{(1)})} \tilde{\pi}_k^{(b_2^{(1)})} \bar{\pi}_k^{(b_2^{(1)})} \tilde{\pi}_k^{(b_2^{(1)})} \bar{\pi}_k^{(b_2^{(1)})} + \cdots$$

$$= \frac{\bar{\pi}_k^{(b_2^{(1)})}}{1 - \tilde{\pi}_k^{(b_2^{(1)})} \bar{\pi}_k^{(b_2^{(1)})}}. \tag{65}$$

Proceeding in the same way for the remaining cases, we get for the full effective vertex

$$\pi_k^{(b_2^{(1)})} = \frac{\bar{\pi}_k^{(b_2^{(1)})} + \tilde{\pi}_k^{(b_2^{(1)})} + \bar{\pi}_k^{(b_2^{(1)})} \tilde{\pi}_k^{(b_2^{(1)})}}{1 - \tilde{\pi}_k^{(b_2^{(1)})} \bar{\pi}_k^{(b_2^{(1)})}}. \tag{66}$$

The structure of the six-point effective vertex may be deduced in the same way. From Eq. (57), we know that the structure equation for six-point effective vertices in the quartic sector is an effective loop built of three effective propagators, hooked together effective four-point vertices. To find the contributions involving bare six-point couplings, we have to list all the possible contractions of an edge e into a typical graph contributing to $\bar{\pi}_k^{b_3^{(1)}}$, in order to build a connected sum of two four-point bare couplings. We have three different ways:

    (i) the edge e is on the effective loop, between two adjacent effective four-point vertices,
    (ii) the edge e is on one of the three effective propagators building the central effective loop, and
    (iii) the edge e is on one of the effective four-point vertices.

Once again, for the last cases, the resulting two-point subgraph provides a contribution to the full two-point function. In the same way, the resulting four-point subgraph provides a contribution to the full four-point function. Neither of these two moves modifies the global structure of the graph: It remains built of three effective four-point vertices connected together with two-point graphs to form an effective loop of length three. The first move, however, modifies the global structure. It generates a six-point vertex to which three hands building effective four-point graphs are hooked. Listing all the allowed configurations, distinguished from their respective symmetry factors, we get

$$\pi_k^{b_3^{(1)}} = \frac{8}{3} (\pi_k^{(b_2^{(1)})})^3 \mathcal{A}_{k,3} + \tilde{\pi}_k^{b_3^{(1)}}, \tag{67}$$

where at this stage $\mathcal{A}_{k,3}$ is not restricted on the quartic sector and where, graphically,

$$\tilde{\pi}_k^{b_3^{(1)}} = $$ $$\tag{68}$$

The relative symmetry factors for each contribution can be easily computed considering the leading-order contributions in the perturbative expansion, and we get

$$\tilde{\pi}_k^{b_3^{(1)}} = Z_6 \lambda_6 (1 - 6\pi_k^{(b_2^{(i)})} \mathcal{A}_{k,2} + 12(\pi_k^{(b_2^{(i)})} \mathcal{A}_{k,2})^2 - 16(\pi_k^{(b_2^{(i)})} \mathcal{A}_{k,2})^3). \tag{69}$$

As a result, from the renormalization conditions $\pi_k^{b_3^{(1)}} = \lambda_6(k)$ and $\pi_k^{b_2^{(1)}} = \lambda_4(k)$, we then deduce the relation between the bare six-point coupling and the effective renormalizable couplings:

$$Z_6 \lambda_6 = \frac{\lambda_6(k) - \frac{4}{3}\lambda_4^3(k)\mathcal{A}_{k,3}}{1 - 6\lambda_4(k)\mathcal{A}_{k,2} + 12(\lambda_4(k)\mathcal{A}_{k,2})^2 - 16(\lambda_4(k)\mathcal{A}_{k,2})^3}. \tag{70}$$

Finally, it is easy to check that the eight-point kernel $\pi^{b_4^{(1)}}$ decomposes as

$$\pi^{b_4^{(1)}} = -2(\bar{\pi}_k^{(b_2^{(i)})})^4 \mathcal{A}_{k,4} + \tilde{\pi}^{b_4^{(1)}}, \tag{71}$$

where, graphically, the last component $\tilde{\pi}^{b_4^{(1)}}$ is given by
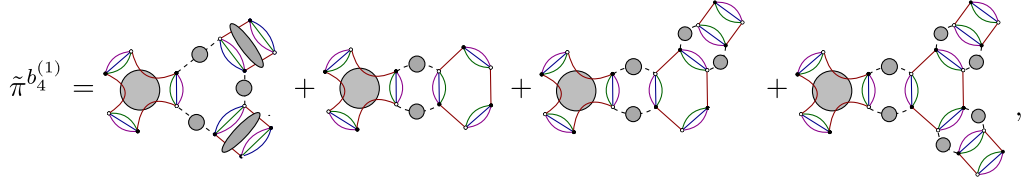
where the effective six-point vertex has been pictured as a gray disk labeled with $\pi^{(b_3)}$, the boundary structure being explicit. Note that we added into $\tilde{\pi}^{b_4^{(1)}}$ the second contribution in (70), to build the first contribution in (72). Computing the relative symmetry factors, using formula (69) to express the bare six-point couplings in term of the effective couplings at scale k, we get finally

$$\tilde{\pi}^{b_4^{(1)}} = \lambda_6(k)\left(24\mathcal{A}_{k,3}\lambda_4^2(k) - \frac{9}{2}\frac{\lambda_6(k) - \frac{4}{3}\lambda_4^3(k)\mathcal{A}_{k,3}}{1 - 6\lambda_4(k)\mathcal{A}_{k,2} + 12(\lambda_4(k)\mathcal{A}_{k,2})^2 - 16(\lambda_4(k)\mathcal{A}_{k,2})^3}\right.$$
$$\left. \times \mathcal{A}_{k,2}(1 - 4\lambda_4(k)\mathcal{A}_{k,2} + 4(\lambda_4(k)\mathcal{A}_{k,2})^2)\right), \tag{73}$$

which closes the system (40). The remaining piece required to complete the set of equations is an equation for Z or, equivalently for the anomalous dimension, that we will fix in the next section.

C. Anomalous dimension and Ward identities

Following the standard definition in the symmetric phase, the *wave function normalization* $Z(k)$ and the *anomalous dimension* $\eta(k)$, completing the set of power-counting renormalizable operators, are defined as follows.

Definition 6: Wave function renormalization and anomalous dimension.—In the symmetric phase, the wave function renormalization is the flow-dependent weight of the Laplacian term and is the derivative expansion of the two-point function $\Gamma_k^{(2)}$:

$$Z(k) := \frac{d}{dp_1^2}\Gamma_k^{(2)}(\vec{p} = \vec{0}). \tag{74}$$

The anomalous dimension $\eta(k)$ is then defined as

$$\eta(k) := \frac{d}{dk}\ln(Z(k)). \tag{75}$$

Note that outside of the symmetric phase, i.e., if we expand around a nonzero vacuum, an additional dependence of Z on

the mean fields may be expected. A standard approximation, already discussed in Ref. [79], is to keep only the leading-order terms of the derivative expansion (DE) for the computation of the loop integrals $L_j(p)$ involved in the system (40). More precisely, we define it as follows.

Definition 7: Leading DE approximation.—In the relevant windows of momenta allowed by the distribution $\dot{r}_k(\vec{p})$, the renormalized effective two-point function $\Gamma_k^{(2)}(\vec{p})$ is approximated by the two first terms of the derivative expansion:

$$\Gamma_k^{(2)}(\vec{p}) = m^2(k) + Z(k)\vec{p}^2. \tag{76}$$

In order to get fixed points, we will consider the *dimensionless and renormalized* couplings, extracting the flow dependence coming from proper canonical dimension and wave function renormalization.

Definition 8: Renormalized and dimensionless couplings.—In the deep UV ($k \gg 1$), the renormalized and dimensionless couplings are defined as

$$m^2 = Z(k)k^2\bar{m}^2, \quad \lambda_4 = Z^2(k)k\bar{\lambda}_4, \quad \lambda_6 = Z^3(k)\bar{\lambda}_6. \tag{77}$$

These are the RG flow equations for these couplings that we have to compute. To this end, we have to get the flow equation for $Z(k)$. From Definition 6, we obtain

$$\dot{Z}(k) = -2\left(\frac{d\pi_k^{(b_2^{(i)})}}{dp^2}(p=0)\right)L_1(0) - 2\lambda_4(k)\left(\frac{dL_1}{dp^2}(p=0)\right). \tag{78}$$

The second piece of the right-hand side may be computed from Definition 7, once the regulator function $r_k(\vec{p})$ is chosen. In order to get a tractable closed system, the first term of the right-hand side has to be computed in terms of the other couplings as well. WT identities come from the unitary invariance of the tensorial interactions and the formal translation invariance of the Lebesgue measure in the path integral (16). Considering an infinitesimal unitary transformation along a single axis on the torus $U(1)^d$, and following the proof given in Refs. [80–83], we may deduce the following theorem.

Theorem 1.—The partition function $\mathcal{Z}_k[J,\bar{J}] =: e^{W_k[J,\bar{J}]}$ of the theory defined by Eq. (16) verifies the WT identity:

$$\sum_{\vec{p}_\perp,\vec{p}'_\perp} \prod_{j\neq 1} \delta_{p_j p'_j} \left\{ [C_s^{-1}(\vec{p}^2) - C_s^{-1}(\vec{p}'^2)]\left[\frac{\partial^2 W_s}{\partial \bar{J}_{\vec{p}'}\partial J_{\vec{p}}} + \bar{M}_{\vec{p}}M_{\vec{p}'}\right] \right.$$
$$\left. - \bar{J}_{\vec{p}}M_{\vec{p}'} + J_{\vec{p}'}\bar{M}_{\vec{p}} \right\} = 0, \tag{79}$$

with $\vec{p}_\perp := (0, p_2, \ldots, p_d) \in \mathbb{Z}^d$ and the mean fields M and $\bar{M}$ defined from Eqs. (22).

Deriving twice with respect to M and $\bar{M}$, and vanishing all the odd vertex functions, required in the symmetric phase, we then deduce a relation between six-point and four-point effective functions. In particular, the dependence with respect to the four-point functions involves a difference between functions having different momenta. Taking the continuum limit, and setting to zero the external momenta, we then deduce the following relation (see Appendix A of Ref. [80]).

Corollary 1: Second zero-momenta WT identity.—In the symmetric phase, the zero-momenta six- and four-point functions satisfy

$$Z_{-\infty}\left[\frac{3}{2}\pi^{(b_3)}\mathcal{L}_1 - 4(\pi^{(b_2)})^2\mathcal{L}_2\right] = -\frac{d}{dp^2}\pi^{(b_2)}(p=0), \tag{80}$$

where $Z_{-\infty}$ denotes the wave-function counterterm, canceling the UV divergences and computed for $k=0$, and where we defined the loop functions $\mathcal{L}_j$ as

$$\mathcal{L}_j := \sum_{\vec{p}_\perp}\left(1 + \frac{\partial\tilde{r}_s(\vec{p}_\perp)}{\partial p_1^2}\right)[G_s(\vec{p}_\perp)]^{j+1}, \quad r_s =: Z_{-\infty}\tilde{r}_s. \tag{81}$$

This relation links the derivative of the four-point effective vertex with the six- and four-point vertices. However, to be exploitable, this relation has to be completed with the WT identity obtained from Eq. (79),

deriving one time with respect to M and $\bar{M}$ and setting to zero the external momenta.

Corollary 2: First zero-momenta WT identity.—In the symmetric phase, the zero-momenta four-point function satisfies

$$2\pi^{(b_2)}Z_{-\infty}\mathcal{L}_1 = -(Z - Z_{-\infty}). \tag{82}$$

To obtain this relation, we used the definition (3.3). Note that, in Eqs. (80) and (82), the derivative of the bare covariance $C_s^{-1}(\vec{p}^2)$ does not involve "boundary terms" coming from the UV cutoff. This is because, to derive these equations, we chose to regularize the divergent integrals using *dimensional regularization*, exploiting the analytic properties of the integrals with respect to the group dimension D. The *continuum limit* in this case is then defined when $D \to 1$.

For our purpose, the interest of the Ward identity (82) is that it allows one to express $Z_{-\infty}$ in terms of effective quantities at scale k:

$$Z_{-\infty} = \frac{Z(k)}{1 - 2\mathcal{L}_1\lambda_4(k)}. \tag{83}$$

Let $\mathcal{L}_j =: \mathcal{A}_{k,j+1} + \frac{1}{Z_{-\infty}}\Delta_j(k)$. Because of the derivative of the regulator $\partial r_k/\partial p^2$ into the last term $\Delta_j(k)$, one expect that it can be computed using the linear differential equation (LDE) approximation given by definition (3.3), as well as the functions $L_j(p)$ defined in (39) and involved in the flow equations (40). In particular, for the choice of the *modified Litim regulator* [52,53]

$$r_k(\vec{p}) = Z(k)(k^2 - \vec{p}^2)\theta(k^2 - \vec{p}^2), \tag{84}$$

the allowed window of momenta is the same for $\dot{r}_k$ and $\partial r_k/\partial p^2$–$\theta(x)$ denoting the standard Heaviside step function. In the rest of this paper, we restrict our attention to this choice, extensively used in the tensor literature and shown to be optimal [52,53] in some practical applications. In the continuum limit, replacing the sums by the corresponding well-defined integrations, we get for Δ_j and L_j

$$\Delta_j(k) = -\frac{Z(k)\Omega_3}{(Zk^2 + m^2)^{j+1}}k^3, \tag{85}$$

$$L_j(p) = Z(k)\Omega_3(k^2 - p^2)^{3/2}\frac{2k^2 + \frac{2}{5}\eta(k)(k^2 - p^2)}{(k^2 Z(k) + m^2(k))^{j+1}}, \tag{86}$$

where $\Omega_3 = \frac{4\pi}{3} \approx 4.19$ denotes the volume of the 3-ball. The computation of the last piece $\mathcal{A}_{k,2}$ is a little bit subtle, the momentum integration being over the full momentum space:

$$\mathcal{A}_{k,j+1} = \sum_{\vec{p}_\perp \in \mathbb{Z}^3} \frac{\theta(k^2 - \vec{p}_\perp^2)}{(\Gamma^{(2)}(\vec{p}_\perp) + r_k(\vec{p}_\perp))^{j+1}}$$

$$+ \sum_{\vec{p}_\perp \in \mathbb{Z}^3} \frac{\theta(\vec{p}_\perp^2 - k^2)}{(\Gamma^{(2)}(\vec{p}_\perp))^{j+1}}. \tag{87}$$

Once again, the first term on the right-hand side can be computed using the LDE approximation, the allowed windows of momenta being the same as for r_k. For the second term, however, the use of this approximation would be an additional approximation, beyond the domain where it can be justified. In Ref. [79], we have shown explicitly that this approximation applied for a superficially divergent integral leads to badly defined results, especially because it introduces a dependence on $Z(k)$ in the deep UV, far away from the scale k. However, in the same discussion, the authors show that, for the superficially convergent integrals, this approximation may be not so bad, because no additional dependence on k is expected on the deep UV. In other words, we assume that the smooth cutoff arising from the convergence of the integrals allows us to use the LDE approximation. We get explicitly

$$\mathcal{A}_{k,j+1} = \frac{\Omega_3 k^3}{(Z(k)k^2 + m^2(k))^{j+1}} + 3\Omega_3 \int_k^\infty \frac{p^2 dp}{(Zp^2 + m^2)^{j+1}}. \tag{88}$$

For any quantity $X(\{\lambda_i\}, m^2)$ depending on the couplings, we denote by $\bar{X}(\{\bar{\lambda}_i\}, \bar{m}^2)$ the corresponding renormalized and dimensionless quantity:

$$X(\{\lambda_i\}, m^2) = k^{d_X} Z^{q_X} \bar{X}(\{\bar{\lambda}_i\}, \bar{m}^2). \tag{89}$$

Defining

$$\mathcal{I}_j(\bar{m}^2) := \int_1^\infty \frac{x^2 dx}{(x^2 + \bar{m}^2)^{j+1}}, \tag{90}$$

we get

$$\bar{\mathcal{A}}_{k,j+1} = -\bar{\Delta}_j + 3\Omega_3 \mathcal{I}_j, \quad \bar{\Delta}_j = -\frac{\Omega_3}{(1 + \bar{m}^2)^{j+1}}, \tag{91}$$

and Eq. (83) is written as

$$Z_{-\infty} = Z(k) \frac{1 - 2\bar{\lambda}_4(k) \frac{\Omega_3}{(1+\bar{m}^2)^2}}{1 - 2\bar{\lambda}_4(k) \bar{\mathcal{A}}_{k,2}}. \tag{92}$$

Introducing this expression into the relation (80), we obtain

$$\frac{\overline{d\pi^{(b_2)}}}{dp^2}(p = 0) = -3\Omega_3 \frac{\frac{3}{2}\bar{\lambda}_6 \mathcal{I}_1(\bar{m}^2) - 4\bar{\lambda}_4^2(\mathcal{I}_2(\bar{m}^2) - \frac{2\bar{\lambda}_4 \Omega_3}{(1+\bar{m}^2)^2} \mathcal{I}_2(\bar{m}^2)) - \frac{\bar{\lambda}_4 \bar{\lambda}_6 \Omega_3}{(1+\bar{m}^2)^2} \mathcal{I}_1(\bar{m}^2)}{1 - 2\bar{\lambda}_4 \bar{\mathcal{A}}_{k,2}}. \tag{93}$$

From Eqs. (93) and (86), and from definition (3.3) giving the anomalous dimension $\eta(k)$, Eq. (78) for $\dot{Z}$ becomes

$$\eta = -2\frac{\overline{d\pi^{(b_2)}}}{dp^2}\Omega_3 \frac{2 + \frac{2}{5}\eta}{(1 + \bar{m}^2)^2} + 2\bar{\lambda}_4 \Omega_3 \frac{3 + \eta}{(1 + \bar{m}^2)^2}. \tag{94}$$

η can be extracted simply as

$$\boxed{\eta = 2\Omega_3 \frac{3\bar{\lambda}_4 - 2\frac{\overline{d\pi^{(b_2)}}}{dp^2}}{(1 + \bar{m}^2)^2 - 2\bar{\lambda}_4 \Omega_3 + \frac{4}{5}\frac{\overline{d\pi^{(b_2)}}}{dp^2}\Omega_3}.} \tag{95}$$

Using Definition 8, we deduce the flow equations for dimensionless and renormalized couplings. We summarize all these results in the following proposition.

Proposition 2.—In the deep UV limit $k \gg 1$, denoting $\beta_2 := \dot{\bar{m}}^2$, $\beta_4 := \dot{\bar{\lambda}}_4$, and $\beta_6 := \dot{\bar{\lambda}}_6$, we have

$$\beta_2 = -(2 + \eta)\bar{m}^2 - 2\Omega_3 \bar{\lambda}_4 \frac{2 + \frac{2}{5}\eta}{(1 + \bar{m}^2)^2}, \tag{96}$$

$$\beta_4 = -(1 + 2\eta)\bar{\lambda}_4 - 3\bar{\lambda}_6 \Omega_3 \frac{2 + \frac{2}{5}\eta}{(1 + \bar{m}^2)^2} + 4\Omega_3 \bar{\lambda}_4^2 \frac{2 + \frac{2}{5}\eta}{(1 + \bar{m}^2)^3}, \tag{97}$$

$$\beta_6 = -3\eta\bar{\lambda}_6 - 4\Omega_3 \overline{\pi_k^{(b_4^{(1)})}} \frac{2 + \frac{2}{5}\eta}{(1 + \bar{m}^2)^2} + 12\Omega_3 \bar{\lambda}_4 \bar{\lambda}_6 \frac{2 + \frac{2}{5}\eta}{(1 + \bar{m}^2)^3}$$

$$- 8\Omega_3 \bar{\lambda}_4^3 \frac{2 + \frac{2}{5}\eta}{(1 + \bar{m}^2)^4}, \tag{98}$$

where $\overline{\pi_k^{(b_4^{(1)})}}$ is given from the structure equation (73) as

$$\overline{\pi_k^{(b_4^{(1)})}} = -2\bar{\lambda}_4^4 \bar{\mathcal{A}}_{k,4} + 3\bar{\lambda}_6 \left(4\bar{\lambda}_4^2 \bar{\mathcal{A}}_{k,3} - \frac{3\bar{\mathcal{A}}_{k,2}}{2} \frac{(\bar{\lambda}_6 - \frac{4}{3}\bar{\lambda}_4^3 \bar{\mathcal{A}}_{k,3})(1 - 4\bar{\lambda}_4 \bar{\mathcal{A}}_{k,2} + 4(\bar{\lambda}_4 \bar{\mathcal{A}}_{k,2})^2)}{1 - 6\bar{\lambda}_4 \bar{\mathcal{A}}_{k,2} + 12(\bar{\lambda}_4 \bar{\mathcal{A}}_{k,2})^2 - 16(\bar{\lambda}_4 \bar{\mathcal{A}}_{k,2})^3}\right). \tag{99}$$

IV. MELONIC PHASE SPACE INVESTIGATIONS

In this section, we investigate the phase space of the RG flow described with the system (96)–(98) in the vicinity of the Gaussian fixed point, where the constraint (108) is trivially satisfied. However, beyond the Gaussian fixed point, we will show that this constraint is violated. Finally, we described the flow on the constrained subspace $\mathcal{E}$.

A. Vicinity of the Gaussian fixed point

Expanding the flow equations (96)–(98) in power of couplings, and keeping only the leading-order contributions in power of couplings, we get a simplified system describing the flow in the vicinity of the Gaussian fixed point, where couplings vanish. For instance, in the exact formula (95), we retain $[\bar{\mathcal{I}}_1(0) = 1]$:

$$\eta \approx 6\Omega_3\bar{\lambda}_4 + 18\Omega_3^2\bar{\lambda}_6. \tag{100}$$

For our analysis, however, we restrict ourselves to the one-loop contributions, which simplifies the incoming analysis. As a consequence, we discard the last term in the right-hand side of the previous equation:
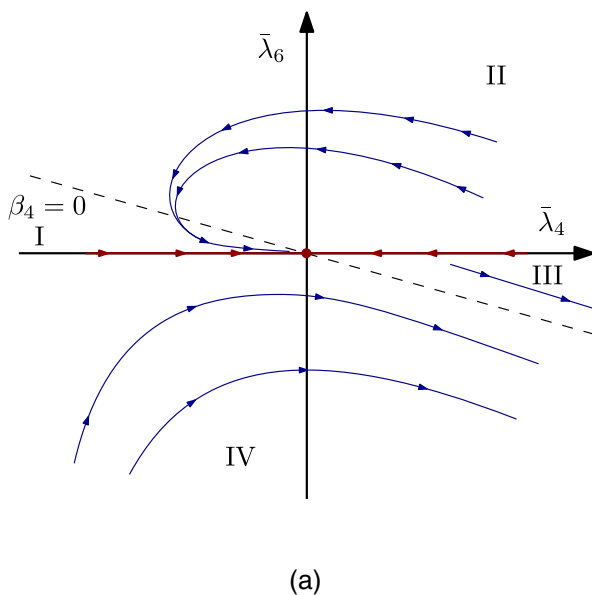
$$\eta \approx 6\Omega_3\bar{\lambda}_4. \tag{101}$$

With this approximation, the relations (96)–(98) reduce to

$$\beta_2 \approx -2\bar{m}^2 - 4\Omega_3\bar{\lambda}_4, \tag{102}$$

$$\beta_4 \approx -\bar{\lambda}_4 - 6\Omega_3\bar{\lambda}_6, \tag{103}$$

$$\beta_6 \approx +6\Omega_3\bar{\lambda}_4\bar{\lambda}_6. \tag{104}$$

The same kind of equations have been obtained for all ϕ^6 models studied in the literature, and extended discussions may be found in Refs. [65–67,70,73]. A qualitative phase portrait may be easily deduced from the system (102). We split the vicinity of the Gaussian fixed point into four regions, I, II, III, and IV as pictured in Fig. 5 below. The boundary between regions I and II on the upper side, and between regions III and IV on the lower side, corresponds to the line defined by the equation $\beta_4 = 0$. The line defined by the equation $\bar{\lambda}_6 = 0$ is the boundary between regions I and IV, on one hand, and between regions II and III, on the other hand.

In the positive neighborhood of region II, where the couplings are both positive, and the beta functions β_4 and β_6 have opposite signs, $\bar{\lambda}_4$ decrease whereas $\bar{\lambda}_6$ increase, and the RG trajectory is then repelled from the horizontal axis and goes to the vertical axis. The maximum for $\bar{\lambda}_6$ arises for $\bar{\lambda}_4 = 0$, that is, when the RG trajectory reaches the vertical axis. Because $\bar{\lambda}_6 > 0$, β_4 remains negative, so that $\bar{\lambda}_4$ pass through the vertical axis and become negative. From now, β_4 and β_6 have the same sign, and the couplings decrease together. The coupling $\bar{\lambda}_6$ goes to zero, whereas the coupling $\bar{\lambda}_4$ becomes more negative. The trajectory then goes far away from the vertical axis and closer to the horizontal axis. Let us focus on the region $\bar{\lambda}_6 \geq 1$. In the vicinity of the vertical axis, $\bar{\lambda}_4$ remains very close to zero, and as soon as $|\bar{\lambda}_4| < 1$, the tangent vectors of the RG trajectory are almost horizontal. The more $|\bar{\lambda}_4|$ grows, the more the tangent vectors become vertical, so that the trajectory goes faster and faster to the horizontal axis, until the trajectory touches the line $\beta_4 = 0$ and passes through, reaching region I. In region I, β_6 remains negative, but β_4
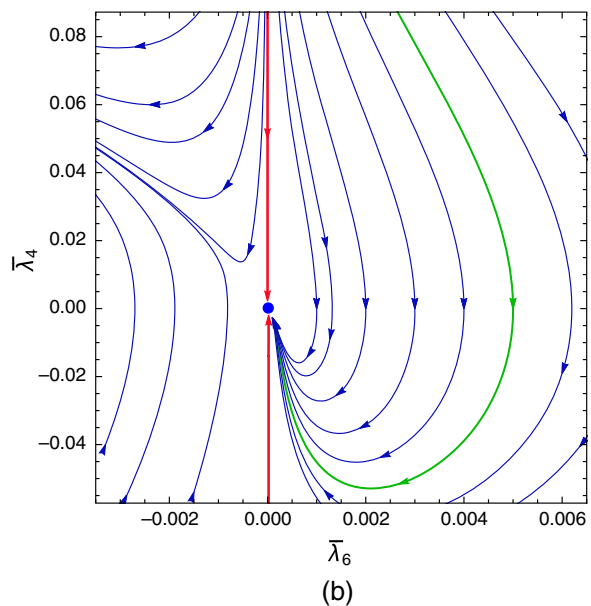

(a)

(b)

FIG. 5. The qualitative picture of the RG trajectories in the plane $(\bar{\lambda}_4, \bar{\lambda}_6)$ (a). The numerical RG flow (b), where the green line corresponds to a typical trajectory on the upper plane, illustrating the discussion.

becomes positive, and then $\bar{\lambda}_4$ begins to grow. At this stage, stuck at the bottom with the red trajectory, the considered trajectory has to reach the Gaussian fixed point.

In Fig. 5(a), we draw a qualitative picture obtained from our previous analysis, and Figs. 5(b) and 6 give the numerical analysis. In a sufficiently small neighborhood in the vicinity of the Gaussian fixed point, the sign of the coupling $\bar{\lambda}_6$ is then conserved along the flow, and the positivity of the initial ϕ^6 action ensures that the starting point has to be in the upper plane, for positive $\bar{\lambda}_6$; our discussion shows that any theory starting in this region must be well defined in the UV.

The additional term is $18\Omega_3^2\bar{\lambda}_6$ in Eq. (100) with respect to the one-loop approximation. Indeed, it introduces a strong attractive term in β_6, $-3 \times 18\Omega_3^2\bar{\lambda}_6^2$ coming from the contribution $-3\eta\bar{\lambda}_6$. Another attractive term $-2 \times 18\Omega_3^2\bar{\lambda}_6^2$ arises from the effective vertex $\overline{\pi_k^{(b_4^{(1)})}}$, so that the equation for β_6 is replaced by

$$\beta_6 \approx +6\Omega_3\bar{\lambda}_4\bar{\lambda}_6 - 5 \times 18\Omega_3^2\bar{\lambda}_6^2$$
$$= 6\Omega_3\bar{\lambda}_6(\bar{\lambda}_4 - 15\Omega_3\bar{\lambda}_6). \qquad (105)$$

This additional attractive term enhances the return of the flow lines toward the horizontal axis. The trajectories in the upper plane $\bar{\lambda}_6 > 0$ escape far away from this axis and do not reach the Gaussian fixed point. Figure 6 represents the numerical RG trajectories in a small neighborhood of the Gaussian fixed point, taking into account this additional term.

These conclusions seem to indicate that the expected UV-protected scenario in the positive region is lost. However, so far from the perturbative region, the behavior of the RG trajectories remains unclear with the perturbative approach. A complementary analysis has to be performed using the full RG equation given by system (96)–(98). Figure 7 provides a numerical integration of the RG equations in the plane $\bar{m}^2 = 0$ for different sizes of the neighborhood surrounding the Gaussian fixed point. In Fig. 7(a), in the vicinity of the Gaussian fixed point, we recover the landscape pictured in Fig. 6(c). Furthermore, far away from the origin in the lower plane $\bar{\lambda}_6 < 0$, the trajectory seems to go away from the horizontal axis. Moreover, following the same arguments used to build Fig. 5(a), the incoming trajectories in the lower plane have no chance to reach the Gaussian fixed point and are repelled before joining it. Figures 7(b) and 7(c) seem to indicate the existence of an attractive vortex in the upper plane $\bar{\lambda}_6 > 0$.
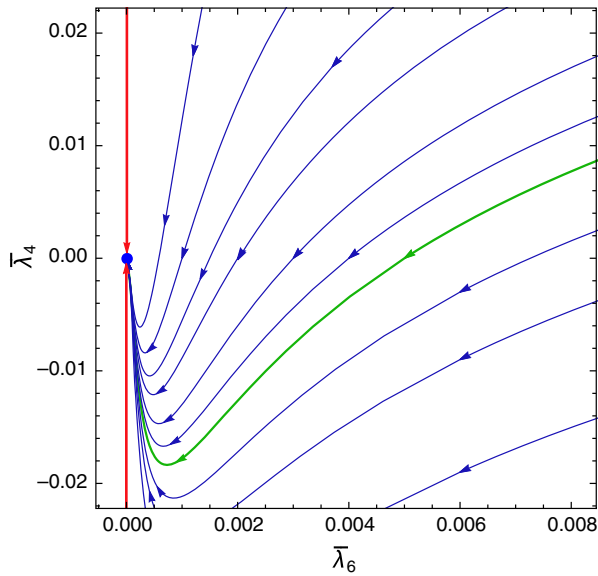

FIG. 6. The qualitative picture of the RG trajectories in the plane $(\bar{\lambda}_4, \bar{\lambda}_6)$. In this figure is the same region of the phase space taking into account the additional term $18\Omega_3^2\bar{\lambda}_6$ in Eq. (100). The relative scales of the figures are chosen to optimize their visibility.
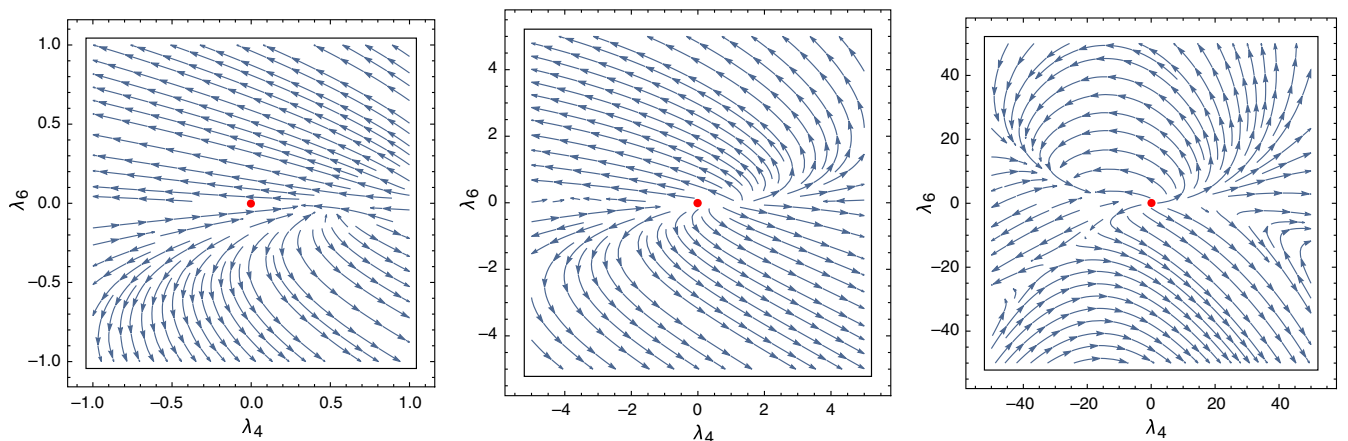

FIG. 7. The behavior of the numerical RG flow in the plane $\bar{m}^2 = 0$, from a very small region in the vicinity of the Gaussian fixed point (a) to a (relatively) large region (c). Again, the scale is adapted to optimize the visibility.

As for the one-loop analysis, the trajectory escaping from the Gaussian region returns to it, attracted along a river reaching the Gaussian fixed point, after a long loop into the phase space. However, we have to be careful. For instance, we have completely neglected the role and the evolution of the mass parameter in this analysis. In the next section, we discuss the existence of a UV-attractive fixed point, completing this picture of the RG flow.

Investigating the solutions of the flow equations in the theory space, we get the nontrivial fixed points (106) and (107), in which we can identify the Wilson-Fisher fixed point FP_2, which was previously announced in our introduction. None of these fixed points are compatible with the Ward identities:

$$FP_1 = (\bar{m}^2 \approx 0.019, \ \bar{\lambda}_4 \approx -0.0019, \ \bar{\lambda}_6 \approx -2.8 \times 10^{-7}),$$
$$(106)$$

$$FP_2 = (\bar{m}^2 \approx -0.3701, \bar{\lambda}_4 \approx 0.34, \bar{\lambda}_6 \approx -0.367). \quad (107)$$

For FP_1 we get the following critical exponent: $(\theta_{11} = 21.63, \theta_{12} = 1.50, \theta_{13} = -0.81)$, which shows that this fixed point have two attractive directions and one repulsive direction in the UV. Note that the value of θ_{11} shows how this attraction behaves very fast in this UV limit. For FP_2 we get $(\theta_{2,1} = 2.8 + 41.7i, \theta_{22} = 2.8 - 41.7i, \theta_{23} = -5.2 + 1.6i)$. Then the fixed point attracts the trajectories in two directions, and the trajectory is repelled by the fixed point in one direction. We will show in the next section that, in the physical subspace of the theory space, all the nontrivial fixed point solution of the constraint flow equation disappeared in the domain with positive values of η.

B. Ward-constrained phase space in the deep UV

In addition to these flow equations (96)–(98), Ward identities introduce a nontrivial constraint, which reduces the dimensionality of the effective flow, from 3 to 2. Indeed, in Eq. (92), $Z_{-\infty}$ does not depend on the running scale k, implying that the right-hand side has to be a constant along the flow. Differentiating both sides with respect to k, this conservation may be translated locally as a constraint binding together the anomalous dimension η and the beta functions $\{\beta_n\}$:

$$\eta \left(1 - \frac{2\bar{\lambda}_4 \Omega_3}{(1+\bar{m}^2)^2} \right) - \frac{2\Omega_3}{(1+\bar{m}^2)^2} \left(\beta_4 - \frac{2\bar{\lambda}_4 \beta_2}{1+\bar{m}^2} \right)$$
$$+ 2\frac{1 - \frac{2\bar{\lambda}_4 \Omega_3}{(1+\bar{m}^2)^2}}{1 - 2\bar{\lambda}_4 \bar{\mathcal{A}}_{k,2}} (\beta_4 \bar{\mathcal{A}}_{k,2} - 2\bar{\lambda}_4 \bar{\mathcal{A}}_{k,3}\beta_2) = 0, \quad (108)$$

where we used $\dot{\bar{\mathcal{A}}}_{k,2} = -2\bar{\mathcal{A}}_{k,3}$. For any fixed point $p = (\bar{m}_*^2, \bar{\lambda}_4^*, \bar{\lambda}_6^*)$, where the beta functions vanish, the previous relation split into two conditions:

$$\eta_* = 0 \quad \text{or} \quad 1 - \frac{2\bar{\lambda}_4^* \Omega_3}{(1+\bar{m}_*^2)^2} = 0. \quad (109)$$

To be physical, any fixed point of the system (96)–(98) has to be verify at least one of these two conditions. In order to get physical flow, we then have to project the RG equations given by the system (96)–(98) into the reduced phase space with the constraint (108). This is the aim of the next section, to investigate this constrained physical phase space. However, before moving on to this investigation, we close this section with some comments about our results. First of all, the constraint given by Eq. (80) has been taken into account in the derivation of η, Eq. (95). As a result, the flow equations given by the system (96)–(98) partially include the constraint coming from the Ward identities. The constraint (92), corresponding to the conservation of $Z_{-\infty}$ along the flow, is the only missing information coming from the Ward identities in the three-dimensional parametric phase space building from the EVE method. The second comment is about the approximation used to compute the integrals. We used the LDE approximation, which is standard for TGFT in the symmetric phase for the computation of the flow equations. However, for the computation of the Ward constraint, and especially for the computation of the convergent integrals $\mathcal{A}_{k,j}$, we used the same approximation, up to the hypothesis that the slow decreasing of the denominator for large $\vec{p}^2$ may support the same approximation as the sharp cutoff coming from Heaviside functions. The consistency of the approximation has been checked in Ref. [76], but not for the same model. As a result, this additional approximation has to be taken into account in our final claims.

Strong violations of the Ward identity (92) can be easily checked for several solutions of the flow equations (96)–(98) (see Ref. [78] for an explicit violation concerning a rank 5 TGFT). In this section, we propose to take into account the constraint (108) along the flow following the strategy described in Ref. [76]. As explained by the authors, the difficulty comes from the definition (68) or (69), inherited from the structure of the melonic diagrams. This definition is too rigid to be conserved on the global phase space without introducing hard singularities. To describe the flow along the constrained subspace $\mathcal{E}$ along which (108) is satisfied, we proceed as follows.

(i) Keeping Eq. (96) for β_2, we replace the definition of β_4 provided by the flow equation by its expression coming from (108):

$$\beta_4 = \frac{4\beta_2 \bar{\lambda}_4 \mathcal{X}(\bar{m}^2, \bar{\lambda}_4) + \eta(\bar{m}^2+1)(2\bar{\mathcal{A}}_{k,2}\bar{\lambda}_4 - 1)((\bar{m}^2+1)^2 - 2\bar{\lambda}_4\Omega_3)}{2(\bar{\mathcal{A}}_{k,2}(\bar{m}^2+1)^3 - (\bar{m}^2+1)\Omega_3)}, \quad (110)$$

where

$$\mathcal{X}(\bar{m}^2, \bar{\lambda}_4) := \Omega_3(2\bar{\mathcal{A}}_{k,2}\bar{\lambda}_4 - 2\bar{\mathcal{A}}_{k,3}(\bar{m}^2 + 1)\bar{\lambda}_4 - 1)$$
$$+ \bar{\mathcal{A}}_{k,3}(\bar{m}^2 + 1)^3. \qquad (111)$$

(ii) Equaling this equation with Eq. (97), we fix the value of $\bar{\lambda}_6$.

(iii) Substituting into Eqs. (93) and (94), we get an explicit expression for the anomalous dimension over $\mathcal{E}$, replacing (95): $\eta_{\mathcal{E}}$.

With this construction, the flow equations and the Ward identity are simultaneously verified along the RG trajectories. Moreover, as λ_6, the higher-order local observables like $\pi_k^{(b_4)}$ are fixed by the flow itself. $\pi_k^{(b_4)}$ is fixed by Eq. (98), the left-hand side being explicitly computed from the explicit dynamical solution for λ_6, and so on. Obviously, our effective equation differs from the unconstrained ones (96)–(98), except in the vicinity of the Gaussian fixed point.

C. Numerical solution of the flow equations in the constraint theory space

The numerical investigation of the flow equations provided from the EVE method [see (96)–(98)] can be given carefully. First of all, by considering the expression (98) we can remark that the quantity $\overline{\pi_k^{(b_4^{(1)})}}$ is specific from the EVE method. This expression does not exist by implementing the truncation as an approximation. In this section, we discuss the solution of the new flow equations taking into account both the Ward constraint and the EVE, with the construction given in Sec. IV B. Then we may compare this analysis with what follows in the last section. Finally, we discuss in detail the asymptotic freedom behavior of this model. After solving the Ward constraint flow equation numerically, we get the Gaussian fixed point $p_0 \approx (\bar{m}^2 = 0, \bar{\lambda}_4 = 0)$, one new point $p_1 \approx (\bar{m}^2 = -0.36, \bar{\lambda}_4 = 0.018)$, and the following critical exponents and eigendirections:

$$p_0: \quad (\theta_{01}, \theta_{02}) \approx (2, 1), \qquad \mathbf{v}_{01} \approx (1, 0),$$
$$\mathbf{v}_{02} \approx (-1, 0.05), \qquad \eta_{p_0} = 0, \qquad (112)$$

$$p_1: \quad (\theta_{11}, \theta_{12}) \approx (1.3, -0.1), \qquad \mathbf{v}_{11} \approx (1, 0.034),$$
$$\mathbf{v}_{12} \approx (1, 0.004), \qquad \eta_{p_1} = 0.10. \qquad (113)$$

For p_0, the trajectory approaches the fixed points and then is UV attractive. In conclusion, our computation enforced our argument about the difficulty to find a physical fixed point compatible with the Ward identities apart from the Gaussian fixed point which represents the trivial solution. Now let us discuss the behavior around the Gaussian fixed point and try to show that the theory is asymptotically free.

Using the constraint flow equation described above, we get asymptotically the following result around the Gaussian fixed point:

$$\beta_2 \approx -2\bar{m}^2 - 4\Omega_3\bar{\lambda}_4, \qquad \beta_4 \approx -\bar{\lambda}_4 - 6\Omega_3\bar{\lambda}_6,$$
$$\bar{\lambda}_6 \approx -4\bar{\lambda}_4^2 \qquad \eta \approx 8\pi\bar{\lambda}_4, \qquad (114)$$

which is in agreement with the results obtained using only the EVE. Note that the β function β_4 will be

$$\beta_4 \approx -\bar{\lambda}_4 + 24\Omega_3\bar{\lambda}_4^2 + \mathcal{O}(\bar{\lambda}_4^2). \qquad (115)$$

Then all values of the coupling tend to zero in the UV limit. The expression of $\beta_4 = \beta_4^0\bar{\lambda}_4 + \beta_4^1\bar{\lambda}_4^2$, and the sign of β_4^0 in the one-loop perturbation computation, show that the theory is asymptotically free in this UV limit; i.e., the flow is attractive around the Gaussian fixed point. The flow diagram around this fixed point is given in Fig. 8 from a numerical integration.

Now consider the fixed point p_1, which has one attractive direction, one repulsive direction, and anomalous dimension $\eta^* = 0.1$. This anomalous dimension enhances the canonical dimension, and following the definition of renormalized couplings, in the vicinity of the non-Gaussian fixed point, the N-point interaction scales with k as $k^{d_N^*}$, with $d_N^* = d_N + \frac{N\eta^*}{2}$, $d_N = 3 - N/2$ being the canonical dimension, i.e., the scaling in the vicinity of the Gaussian fixed point. Obviously, d_N^* is negative for $N > 6$, showing qualitatively that the list of relevant couplings is the same as in the perturbative regime. The values for the critical exponents are in accordance with this argument, in favor of the reliability of our conclusions.
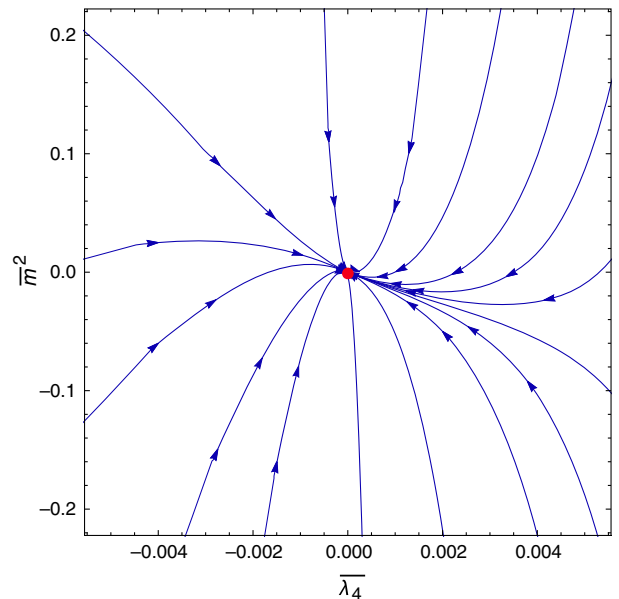

FIG. 8. The behavior of the numerical RG flow in the vicinity of the non-Gaussian fixed points in the space $\mathcal{E}$.

V. CONCLUSION

In this work, we build a solution to the nonperturbative functional renormalization group equation applied to a tensorial just-renormalizable ϕ_4^6 model, merging together the effective vertex expansion and the Ward-Takahashi identities. In the strictly local potential approximation, these identities can be translated as a nontrivial relation between beta functions along the flow. Focussing only on the nonbranching sector, we prove asymptotic freedom (already conjectured in Ref. [36]), as well as the existence of two non-Gaussian fixed points using the standard EVE method, and, in particular, the existence of a UV-attractive fixed point matching with the heuristic arguments given in the introduction. These nontrivial solution of the renormalization group equation, however, are not compatible with the strong Ward constraint. Investigating the fully constrained space $\mathcal{E}$, connected to the Gaussian region, we discovered the existence of a new nontrivial fixed point, with one attractive and one repulsive direction. The characteristics of this fixed point seem to be in accordance with our approximations, in particular, in regard to the derivative expansion around marginal operators. Obviously, deep investigations have to be provided to improve this result, especially about interactions with disconnected boundaries or derivative couplings, sorting out to the strictly local potential approximation.

[1] C. Pagani and M. Reuter, Background independent quantum field theory and gravitating vacuum fluctuations, arXiv:1906.02507.

[2] G. Chirco, A. Goeßmann, D. Oriti, and M. Zhang, Group field theory and holographic tensor networks: Dynamical corrections to the Ryu-Takayanagi formula, arXiv:1903.07344.

[3] D. Oriti, Group field theory and simplicial quantum gravity, Classical Quantum Gravity **27,** 145017 (2010).

[4] D. Oriti, Levels of spacetime emergence in quantum gravity, arXiv:1807.04875.

[5] A. Baratin and D. Oriti, Ten questions on group field theory (and their tentative answers), J. Phys. Conf. Ser. **360,** 012002 (2012).

[6] D. Oriti, The group field theory approach to quantum gravity: Some recent results, AIP Conf. Proc. **1196,** 209 (2009).

[7] A. Ashtekar, M. Reuter, and C. Rovelli, From general relativity to quantum gravity, arXiv:1408.4336.

[8] C. Rovelli, Loop quantum gravity, Living Rev. Relativity **1,** 1 (1998).

[9] C. Rovelli and P. Upadhya, Loop quantum gravity and quanta of space: A primer, arXiv:gr-qc/9806079.

[10] C. Rovelli, Quantum gravity, Scholarpedia **3,** 7117 (2008).

[11] C. Rovelli, Zakopane lectures on loop gravity, Proc. Sci., QGQGS2011 (**2011**) 003 [arXiv:1102.3660].

[12] C. Rovelli, Loop quantum gravity: The first twenty five years, Classical Quantum Gravity **28,** 153002 (2011).

[13] J. Ambjorn, Z. Burda, J. Jurkiewicz, and C. F. Kristjansen, Quantum gravity represented as dynamical triangulations, Acta Phys. Pol. B **23,** 991 (1992).

[14] J. Ambjorn, Quantum gravity represented as dynamical triangulations, Classical Quantum Gravity **12,** 2079 (1995).

[15] J. Ambjørn, A. Görlich, J. Jurkiewicz, and R. Loll, Quantum gravity via causal dynamical triangulations, arXiv:1302.2173.

[16] A. Connes and J. Lott, Particle models and noncommutative geometry (expanded version), Nucl. Phys. B, Proc. Suppl. **18,** 29 (1991).

[17] J. Aastrup and J. M. Grimstrup, Intersecting connes noncommutative geometry with quantum gravity, Int. J. Mod. Phys. A **22,** 1589 (2007).

[18] A. Perez, Spin foam quantization of SO(4) Plebanski's action, Adv. Theor. Math. Phys. **5,** 947 (2001); Erratum, Adv. Theor. Math. Phys. **6,** 593(E) (2002).

[19] D. Oriti, A quantum field theory of simplicial geometry and the emergence of spacetime, J. Phys. Conf. Ser. **67,** 012052 (2007).

[20] M. de Cesare, A. G. A. Pithis, and M. Sakellariadou, Cosmological implications of interacting group field theory models: Cyclic Universe and accelerated expansion, Phys. Rev. D **94,** 064051 (2016).

[21] S. Gielen and L. Sindoni, Quantum cosmology from group field theory condensates: A review, SIGMA **12,** 082 (2016).

[22] S. Gielen and D. Oriti, Cosmological perturbations from full quantum gravity, Phys. Rev. D **98,** 106019 (2018).

[23] S. Gielen and D. Oriti, Quantum cosmology from quantum gravity condensates: Cosmological variables and lattice-refined dynamics, New J. Phys. **16,** 123004 (2014).

[24] S. Gielen, D. Oriti, and L. Sindoni, Homogeneous cosmologies as group field theory condensates, J. High Energy Phys. 06 (2014) 013.

[25] S. Gielen, Inhomogeneous universe from group field theory condensate, J. Cosmol. Astropart. Phys. 02 (2019) 013.

[26] D. Colosi and C. Rovelli, What is a particle?, Classical Quantum Gravity **26,** 025002 (2009).

[27] R. Gurau, The complete 1/N expansion of colored tensor models in arbitrary dimension, Ann. Henri Poincaré **13,** 399 (2012).

[28] R. Gurau and V. Rivasseau, The 1/N expansion of colored tensor models in arbitrary dimension, Europhys. Lett. **95,** 50004 (2011).

[29] R. Gurau and J. P. Ryan, Melons are branched polymers, Ann. Henri Poincaré **15,** 2085 (2014).

[30] R. Gurau, Colored group field theory, Commun. Math. Phys. **304,** 69 (2011).

[31] R. Gurau and J. P. Ryan, Colored tensor models–A review, SIGMA **8,** 020 (2012).

[32] R. Gurau, The 1/N expansion of colored tensor models, Ann. Henri Poincaré **12,** 829 (2011).

[33] P. Di Francesco, P. H. Ginsparg, and J. Zinn-Justin, 2-D gravity and random matrices, Phys. Rep. **254**, 1 (1995).

[34] J. B. Geloun and V. Rivasseau, A renormalizable 4-dimensional tensor field theory, Commun. Math. Phys. **318**, 69 (2013).

[35] J. B. Geloun and D. O. Samary, 3D tensor field theory: Renormalization and one-loop β-functions, Ann. Henri Poincaré **14**, 1599 (2013).

[36] J. B. Geloun, Two and four-loop β-functions of rank 4 renormalizable tensor field theories, Classical Quantum Gravity **29**, 235011 (2012).

[37] J. B. Geloun and E. R. Livine, Some classes of renormalizable tensor models, J. Math. Phys. (N.Y.) **54**, 082303 (2013).

[38] J. B. Geloun and V. Bonzom, Radiative corrections in the Boulatov-Ooguri tensor model: The 2-point function, Int. J. Theor. Phys. **50**, 2819 (2011).

[39] V. Lahoche, D. Oriti, and V. Rivasseau, Renormalization of an Abelian tensor group field theory: Solution at leading order, J. High Energy Phys. 04 (2015) 095.

[40] S. Carrozza, D. Oriti, and V. Rivasseau, Renormalization of tensorial group field theories: Abelian U(1) models in four dimensions, Commun. Math. Phys. **327**, 603 (2014).

[41] D. O. Samary and F. Vignes-Tourneret, Just renormalizable TGFT's on $U(1)^d$ with gauge invariance, Commun. Math. Phys. **329**, 545 (2014).

[42] S. Carrozza, D. Oriti, and V. Rivasseau, Renormalization of a SU(2) tensorial group field theory in three dimensions, Commun. Math. Phys. **330**, 581 (2014).

[43] K. G. Wilson, Renormalization group and critical phenomena. 1. Renormalization group and the Kadanoff scaling picture, Phys. Rev. B **4**, 3174 (1971).

[44] K. G. Wilson, Renormalization group and critical phenomena. 2. Phase space cell analysis of critical behavior, Phys. Rev. B **4**, 3184 (1971).

[45] C. Wetterich, Exact evolution equation for the effective potential, Phys. Lett. B **301**, 90 (1993).

[46] C. Wetterich, Average action and the renormalization group equations, Nucl. Phys. **B352**, 529 (1991).

[47] C. Wetterich, Effective average action in statistical physics and quantum field theory, Int. J. Mod. Phys. A **16**, 1951 (2001).

[48] D. Schnoerr, I. Boettcher, J. M. Pawlowski, and C. Wetterich, Error estimates and specification parameters for functional renormalization, Ann. Phys. (Amsterdam) **334**, 83 (2013).

[49] J. Berges, N. Tetradis, and C. Wetterich, Nonperturbative renormalization flow in quantum field theory and statistical physics, Phys. Rep. **363**, 223 (2002).

[50] B. Delamotte, An introduction to the nonperturbative renormalization group, Lect. Notes Phys. **852**, 49 (2012).

[51] N. Tetradis and D. F. Litim, Analytical solutions of exact renormalization group equations, Nucl. Phys. **B464**, 492 (1996).

[52] D. F. Litim, Optimization of the exact renormalization group, Phys. Lett. B **486**, 92 (2000).

[53] D. F. Litim, Derivative expansion and renormalization group flows, J. High Energy Phys. 11 (2001) 059.

[54] S. Nagy, Lectures on renormalization and asymptotic safety, Ann. Phys. (N.Y.) **350**, 310 (2014).

[55] J. P. Blaizot, R. Mendez-Galain, and N. Wschebor, Non perturbative renormalisation group and momentum dependence of n-point functions. I, Phys. Rev. E **74**, 051116 (2006).

[56] J. P. Blaizot, R. Mendez-Galain, and N. Wschebor, Non perturbative renormalization group and momentum dependence of n-point functions. II, Phys. Rev. E **74**, 051117 (2006).

[57] N. Defenu, P. Mati, I. G. Marian, I. Nandori, and A. Trombettoni, Truncation effects in the functional renormalization group study of spontaneous symmetry breaking, J. High Energy Phys. 05 (**2015**) 141.

[58] S. Akiyama, Y. Kuramashi, T. Yamashita, and Y. Yoshimura, Phase transition of four-dimensional Ising model with higher-order tensor renormalization group, Phys. Rev. D **100**, 054510 (2019).

[59] A. D. Pereira, Quantum spacetime and the renormalization group: Progress and visions, arXiv:1904.07042.

[60] J. F. Mathiot, The renormalization group equations revisited, Int. J. Mod. Phys. A **33**, 1830024 (2018).

[61] A. G. A. Pithis and J. Thürigen, Phase transitions in group field theory: The Landau perspective, Phys. Rev. D **98**, 126006 (2018).

[62] J. B. Geloun, R. Martini, and D. Oriti, Functional renormalization group analysis of tensorial group field theories on $\mathbb{R}^d$, Phys. Rev. D **94**, 024017 (2016).

[63] J. B. Geloun, R. Martini, and D. Oriti, Functional renormalization group analysis of a tensorial group field theory on $\mathbb{R}^3$, Europhys. Lett. **112**, 31001 (2015).

[64] D. Benedetti, J. B. Geloun, and D. Oriti, Functional renormalisation group approach for tensorial group field theory: A Rank-3 model, J. High Energy Phys. 03 (2015) 084.

[65] S. Carrozza, Discrete renormalization group for SU(2) tensorial group field theory, Ann. Inst. Henri. Poincaré D **2**, 49 (2015).

[66] S. Carrozza and V. Lahoche, Asymptotic safety in three-dimensional SU(2) group field theory: Evidence in the local potential approximation, Classical Quantum Gravity **34**, 115004 (2017).

[67] S. Carrozza, V. Lahoche, and D. Oriti, Renormalizable group field theory beyond melonic diagrams: An example in rank four, Phys. Rev. D **96**, 066007 (2017).

[68] A. Eichhorn, T. Koslowski, and A. D. Pereira, Status of background-independent coarse-graining in tensor models for quantum gravity, Universe **5**, 53 (2019).

[69] J. B. Geloun, T. A. Koslowski, D. Oriti, and A. D. Pereira, Functional renormalization group analysis of rank 3 tensorial group field theory: The full quartic invariant truncation, Phys. Rev. D **97**, 126018 (2018).

[70] V. Lahoche and D. O. Samary, Functional renormalization group for the U(1)-T_5^6 tensorial group field theory with closure constraint, Phys. Rev. D **95**, 045013 (2017).

[71] D. Benedetti and V. Lahoche, Functional renormalization group approach for tensorial group field theory: A Rank-6 model with closure constraint, Classical Quantum Gravity **33**, 095003 (2016).

[72] D. Benedetti, R. Gurau, and S. Harribey, Line of fixed points in a bosonic tensor model, J. High Energy Phys. 06 (2019) 053.

[73] S. Carrozza, Group field theory in dimension $4 - \epsilon$, Phys. Rev. D **91**, 065023 (2015).

[74] D. Benedetti and N. Delporte, Phase diagram and fixed points of tensorial Gross-Neveu models in three dimensions, J. High Energy Phys. 01 (2019) 218.

[75] D. Benedetti and R. Gurau, Phase transition in dually weighted colored tensor models, Nucl. Phys. **B855,** 420 (2012).

[76] V. Lahoche and D. O. Samary, Ward-constrained melonic renormalization group flow, arXiv:1904.05655.

[77] V. Lahoche and D. O. Samary, Progress in the solving nonperturbative renormalization group for tensorial group field theory, Universe **5,** 86 (2019).

[78] V. Lahoche and D. O. Samary, Ward identity violation for melonic T^4-truncation, Nucl. Phys. **B940,** 190 (2019).

[79] V. Lahoche and D. O. Samary, Nonperturbative renormalization group beyond the melonic sector: The effective vertex expansion method for group fields theories, Phys. Rev. D **98,** 126010 (2018).

[80] V. Lahoche and D. O. Samary, Unitary symmetry constraints on tensorial group field theory renormalization group flow, Classical Quantum Gravity **35,** 195006 (2018).

[81] D. O. Samary, Closed equations of the two-point functions for tensorial group field theory, Classical Quantum Gravity **31,** 185005 (2014).

[82] D. O. Samary, C. I. Pérez-Sanchez, F. Vignes-Tourneret, and R. Wulkenhaar, Correlation functions of a just renormalizable tensorial group field theory: The melonic approximation, Classical Quantum Gravity **32,** 175012 (2015).

[83] V. Lahoche, From perturbative to nonperturbative renormalizationin tensorial group field theories, Ph. D. thesis, https://tel.archives-ouvertes.fr/tel-01476110.